UBY ILL – Lending
TN: 502509 Pages: 33 pages ARIEL
TXA
Call (801) 422-8648 for resends.

ILLiad TN: 502509

Call #: Q 1 .A3 U64x

Location: 2ND

Journal Title: Technical report - Snow, Ice and Permafrost Research Establishment. **ISSN:**

Volume: **Issue:** Research Report 46
Month/Year: 1959 **Pages:** 33 pages **ARIEL**

Article Author: Snow, Ice, and Permafrost Research Establishment (U.S.)
Article Title: Nakaya U.; Visco-elastic properties of snow and ice in the Greenland ice cap

ILL Number: 4009998

Lending String:
*UBY,CAI,IWA,LDL,UDI

Patron: santos, juan

Borrower: TXA
Texas A&M University
TAMU Libraries -Interlibrary Services
5000 TAMUS
College Station, TX 77843-5000
Fax: 979-862-4759
Ariel: 165.91.220.14
Odyssey:

BYU

BRIGHAM YOUNG UNIVERSITY

Harold B. Lee Library
Interlibrary Loan
Copy Center

For Ariel Receipt Problems:
Phone: 801-422-8648
Fax: 801-422-0464
Ariel: 128.187.229.251
Email: barbara_allred@byu.edu

Ariel Problem Report

If you have experienced a problem in the delivery of the requested item, please contact us within **Five Business Days** with the following information:

ILL#: _____
Your OCLC Symbol: _____
Date of Receipt: _____

Please specify if:

_____ Pages were Missing – pp._____ to _____
_____ Edges were Cut Off – pp._____ to _____
_____ Illegible Copy – Resend entire item
_____ Wrong Article Sent
_____ Other (Explain): _____

VISCO-ELASTIC PROPERTIES OF SNOW AND ICE IN THE GREENLAND ICE CAP

by

Ukichiro Nakaya

1. Introduction

In recent years the problem of the visco-elastic nature of snow and ice has been taken up by many physicists and glaciologists. Among them the work of Glen and Perutz (1954), Glen (1952), Landauer (1955), Jellinek and Brill (1956), and deQuervain (1946) may be considered to be up to date and detailed. They used the static method and measured the stress and strain relation as well as the rate of creep by applying various stresses to the specimen. On the other hand it is also desirable to study the visco-elastic properties of snow and ice by the sonic method. Kuroiwa and Yamaji (1954; 1956) have measured Young's modulus and viscosity of snow using a transverse vibration method. The results obtained by this method seemed successful and the author decided to use a similar instrument to begin investigation of visco-elastic properties of snow and ice in the Greenland Ice Cap. Torsional vibration, usually used for metals, is difficult to apply for ice or snow; the sample cannot be made as thin because of the rapid evaporation of ice, and clamping of a snow or ice sample is very difficult.

The investigations were carried out in connection with Corps of Engineers Projects 22.2 and 25.2 as a part of the USA SIPRE Greenland program in the summer of 1957. The author brought a newly designed visco-elastic meter of portable type to Greenland, and spent about 40 days at TUTO, 14 miles inland from Thule, and at Site 2, 220 miles east of Thule and near 78°N latitude and 7000 ft elevation. At TUTO the samples tested were taken from the walls of the ice tunnel which had been dug into the edge of the ice cap near TUTO. At Site 2, samples of snow and ice from various depths of the ice cap were tested.

Some samples of tunnel ice were brought back to the USA SIPRE laboratory in Wilmette, Illinois and studied in more detail. The results of all these experiments are described in this report. The experimental data are tabulated in the appendix.

2. Principle of measuring the visco-elastic nature of snow and ice by the vibration method

The principle of measuring Young's modulus is based on the resonance vibration of the sample, which is made in the form of a rectangular bar. The solution of the flexural vibration of a bar was obtained by Lord Rayleigh (Strutt, 1925) for elastic vibration without internal viscosity. The frequency of the vibration is

$$f = \frac{kbm^2}{2\pi\ell^2}$$

where ℓ is the length of the bar; b the velocity of sound in the material, that is $\sqrt{E/\rho}$; E is Young's modulus and ρ the density of the material. m is an abstract number and its value is 4.730 for the fundamental mode, 7.853 for the second mode, and corresponding values for the other modes. k is the radius of gyration of the section about an axis perpendicular to the plane of bending; $k^2 = h^2/12$ for a rectangular bar. h is the thickness of the bar; the width is not introduced in this equation. Young's modulus, therefore, is obtained for a rectangular bar by

$$E = \frac{48\pi^2\ell^4\rho}{m^4h^2}f^2. \qquad (1)$$

In plastic materials where the internal viscosity is effective, the energy dissipates because of the phase lag of the strain behind the stress. The stress-strain relation is expressed in complex numbers, and is studied in detail in the field of high polymers.

When the stress σ undergoes a harmonic motion with the angular frequency ω, the strain γ lags behind the stress by the loss angle δ.

$$\sigma = \sigma_0 \sin \omega t,$$
$$\gamma = \gamma_0 \sin (\omega t - \delta).$$

The stress-strain relation is conveniently expressed by complex numbers.

$$\sigma^* = G^* \gamma^*. \tag{2}$$

G^*, which corresponds to Young's modulus in the case of purely elastic materials, is called the complex shear modulus.

$$G^* = G_1 + iG_2. \tag{3}$$

The real part G_1 is called the storage modulus and is related to the elasticity of the material. The imaginary part G_2, the loss modulus, is a constant related to the internal friction. The dissipated energy is expressed by $\tan \delta$, which is called the loss factor or the mechanical loss.

$$\tan \delta = G_1 / G_2. \tag{4}$$

The loss factor $\tan \delta$ is measured experimentally, but some artificial model must be introduced in order to relate this loss factor to the internal viscosity. The relation between the loss factor and the viscosity η is different for different models.

The simplest model to express the retarded elastic behavior is the Voigt model; a spring with E_1 and a dashpot with η_1 are combined in parallel. The equation of motion is

$$\dot{\gamma} + \frac{1}{\tau} \gamma = \frac{1}{\eta_1} \sigma, \tag{5}$$

in which $\tau = \eta_1 / E_1$ is the retardation time. The solution is

$$G^* = G_1 + iG_2 = E_1 + i\omega\eta_1. \tag{6}$$

G_1 is the Young's modulus of the spring, and G_2 is directly proportional to the viscosity of the dashpot. The loss factor is proportional to the viscosity.

$$\tan \delta = \omega\eta_1 / E_1. \tag{7}$$

For the Maxwell model, which is a combination of a spring with E_2 and a dashpot with η_2 in series, the equation of motion is

$$\dot{\sigma} + \frac{1}{\tau'} \sigma = E_2 \dot{\gamma}, \tag{8}$$

in which $\tau' = \eta_2 / E_2$ is the relaxation time. The solution is

$$G^* = E' + i\omega\eta',$$

$$E' = E_2 \frac{\omega^2 \tau'^2}{1+\omega^2 \tau'^2}, \quad \eta' = \frac{E_2 \tau'}{1+\omega^2 \tau'^2},$$

or

$$E' = E_2 \left(1 + \frac{1}{\omega^2 \tau'^2}\right)^{-1}, \quad \eta' = \frac{1}{\eta_2} \frac{E_2^2}{\omega^2} \left(1 + \frac{1}{\omega^2 \tau'^2}\right)^{-1}. \tag{9}$$

$$\tan \delta = E_2 / \omega\eta_2. \tag{10}$$

In this case the loss factor is inversely proportional to the viscosity, contrary to the case of Voigt model. The interpretation of the mechanical loss in terms of viscosity is quite different for different models. On the other hand, the term representing the elasticity is almost the same for the two models. Eq 6 and 9 show that the equivalent Young's modulus is the same as that of the model spring in the Voigt model, and almost the same with some correction in the Maxwell model.

The solution of the lateral vibration of a rectangular bar with damping was obtained by Yosida (1956). The vibration attenuates with the damping coefficient λ.

$$A = A_0 e^{-\lambda t} \sin \omega t. \tag{11}$$

λ and ω are expressed by

$$\omega^2 + \lambda^2 = \frac{m^4 h^2 E}{12 \ell^4 \rho} . \tag{12}$$

In most cases λ^2 can be neglected with respect to ω^2, and eq 12 becomes eq 1. The loss factor is expressed by

$$\tan \delta = 2\lambda / \omega . \tag{13}$$

The amplitude decrease was checked at various temperatures with C1 and C2 ice (Table II). The logarithm of amplitude decreases linearly with time (Fig. 1) and the value of λ is determined by the slope of the straight line.

By measuring λ from the oscillogram, $\tan \delta$ is calculated by eq 13, and the coefficient of viscosity is given by

$$\eta_1 = \frac{E_1 \tan \delta}{\omega} \text{ for the Voigt model} \qquad \eta_2 = \frac{E_2}{\omega \tan \delta} \text{ for the Maxwell model.} \tag{14}$$

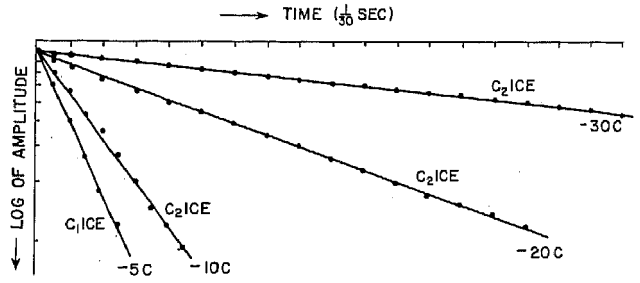

Figure 1. Amplitude decrease at various temperatures.

The viscosity expressed by eq 14 is that of the dashpot model, and is different for different models. As not much is known about the mechanism of dissipation of energy the value of viscosity thus obtained has little physical meaning, but it will serve as a clue for the study of the mechanism of energy dissipation. The value of $\tan \delta$, which expresses the mechanical loss due to internal viscosity, is determined experimentally and does not depend on the type of model used. In this paper, therefore, $\tan \delta$ was used mostly to describe the viscous nature of the sample. The dissipated energy ΔW due to visco-elastic loss in the material is

$$\Delta W = \pi \tan \delta \, G_1 \gamma_0^2 \tag{15}$$

where G_1 is the Young's modulus for the Voigt model and is approximate to it for the Maxwell model. For a given amplitude, $\tan \delta$ is exactly or nearly proportional to the amount of dissipated energy per cycle.

3. Experimental method for determination of visco-elastic properties of snow and ice

A schematic diagram of the instrument used in Greenland is shown in Figure 2. The sample of snow or ice, S, is cut in a rectangular bar, and is supported on two strings stretched horizontally. The position of the string should coincide with the nodal point of the vibration, but a deviation of a few mm does not affect the result

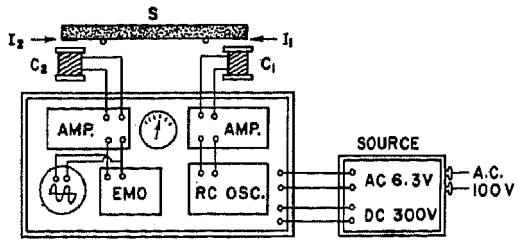

Figure 2. Schematic diagram of the portable visco-elastic meter..

appreciably. The nodal point is 0.22 ℓ from each end for the fundamental mode. A small thin iron plate is frozen to each end of the bar; I_1 and I_2. The thinner the plate the better; the vibrating plate of a telephone receiver is used for this. The ordinary RC oscillator (Resistance-capacitance tuned oscillator) is connected to the exciting coil C_1 through an amplifier which gives rise to the forced oscillation of the bar. The frequency of the exciting current is changed continuously by a variable condenser. When the frequency coincides with that of the resonance vibration of the bar, the induced current in coil C_2 due to the vibration of iron plate I_2 becomes maximum. This induced current is amplified and recorded on an electromagnetic oscillograph. Consolidated Engineering Corporation's Type 5-118 with paper speed of 3 in./sec was used for this purpose. A 60-cycle generator was used as the time mark. A cathode ray oscilloscope was used for visual observation of the wave form and the amplitude. The resonance frequency was found at the maximum of amplitude and measured on the dial, which had been calibrated with the 60-cycle generator.

In this series of experiments, only the fundamental vibration was measured. For soft snow the third mode of flexural vibrations sometimes takes place, with 4 nodal points. In this case the supporting string is near the loop of the wave, and the string cuts easily into the snow sample. If this happens, the sample is damaged. The fifth mode of flexural vibration with 6 nodal points is also likely to occur. The position of the string is near the nodal point in this case, and sometimes this is mistaken for the fundamental vibration. The modes of flexural vibration with odd numbers of modes, 3 and 5, are difficult to obtain for soft snow.

After the resonance frequency was measured, the exciting current was short-circuited and the amplitude decrease was recorded on the oscillograph. Several examples are shown in Figures 40-43. The amplitude decreases exponentially with time. The energy loss is calculated from the slope of the straight line shown in Figure 1. In most cases the attenuation constant was calculated by measuring the time required for the amplitude to decrease to $\frac{1}{3}$ of the initial value. Except for soft snow, the dimensions of samples were usually $\ell \sim 20$-25 cm, h $\sim$ 5-10 mm, b $\sim$ 2 cm, and the resonance frequency was between about 200 and 300 cps. For the study of frequency dependence, the frequency was varied in the range of 150 and 650 cps.

4. Visco-elastic properties of tunnel ice

Ice samples from various portions of the ice tunnel were tested. The samples contained air bubbles and air columns trapped in the ice. Five types of ice samples (Table I) were tested in a room constructed in the tunnel. The air temperature was almost constant at nearly -5C, but sometimes went up to about -4C. Eighteen specimens, T1 through T18, were tested. Some of the samples (Table II) were brought back to the USA SIPRE laboratory, by the aid of dry ice, and a more detailed investigation was carried out in the cold rooms at various temperatures.

A1 and A2 (Fig. 3) are superimposed ice, formed by alternate thawing and freezing of drifted wind-packed snow on the lee side of the terminal moraine. This is not ice from inside the ice cap but is found near the portal of the tunnel. It contains a few small bubbles, is fairly transparent, and looks bluish in situ. Its density is nearly that of pure ice. B1 and B2 (Fig. 4) belong to a type which is characterized by air columns and elongated bubbles, which are well oriented in one direction. Ice samples of this type are sometimes different in nature, even if they are taken from one location. The density varies between 0.905 and 0.910 g/cm^3. For detailed investigation, this type must be classified into several subgroups. E1 and E2 were taken at one spot; E1 was taken horizontally and E2 vertically. This ice contained

Table I. Ice samples tested in the tunnel.

No.	ρ(g/cm^3)	Nature of ice	Butkovich notation (1959)
A1	0.916	Clear (superimposed ice)	MP5
B1	0.905 - 0.908	Air columns and elongated bubbles	MP2
D	0.9125	Air bubbles and dirt bands	MP4
E1	0.910	Many small bubbles	MP4
E2	0.913	Many small bubbles	MP4

Table II. Ice samples tested in the USA SIPRE laboratory.

No.	ρ(g/cm^3)	Nature of ice	Butkovich notation (1959)
I	0.917	Commercial ice without bubbles	---
A2	0.915	Clear (superimposed ice)	MP5
B2	0.910	Air columns and elongated bubbles	MP2
C1	0.911	Many very small bubbles; 680 ft from entrance of tunnel	
C2	0.910	Many very small bubbles; 680 ft from entrance of tunnel	

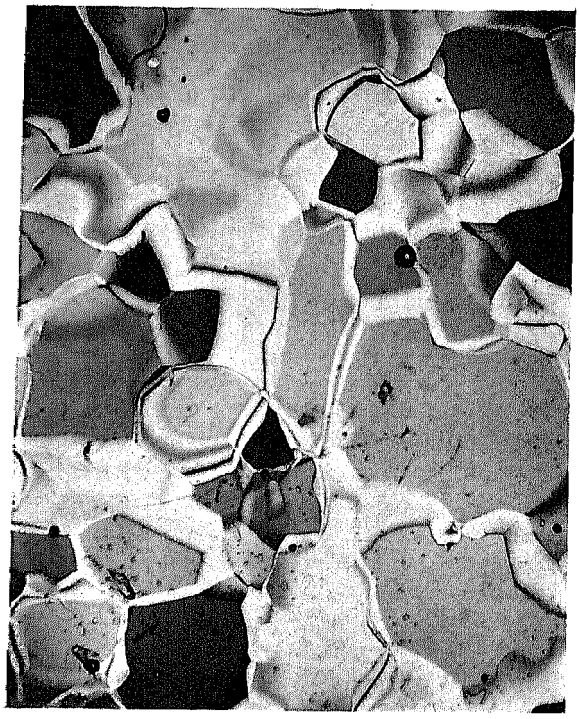

Figure 3. A2 ice, superimposed ice, = 0.915 g/cm^3, x 10.under crossed polaroids.

Figure 4. B2 ice, ice-cap ice, ρ = 0.910 g/cm^3, x 10.

many small bubbles and showed a milky appearance with a slightly bluish tint. The bubbles are not spherical and show a tendency of orientation in one direction. Judging from the shape and size of the bubbles, E ice is considered to be much older than B ice. Bands of fine silt or clay particles are sometimes observed in the ice, near E ice. This ice with dirt bands is called D ice. The density of D ice is nearly the same as that

Figure 5. C1 ice, 680 ft from tunnel portal; $\rho = 0.911$ g/cm^3 x 10.

Figure 6. C2 ice, 680 ft from tunnel portal; $\rho = 0.910$ g/cm^3 x 10.

of E ice, but its Young's modulus is higher. C1 and C2 were taken 680 ft from the portal of the ice tunnel (Fig. 5, 6). The bubbles are very small and abundant. Some of them are seen on the grain boundaries, but most of them are within the grain. The general appearance of the bubbles is ovoid and a slight tendency of orientation is observed.

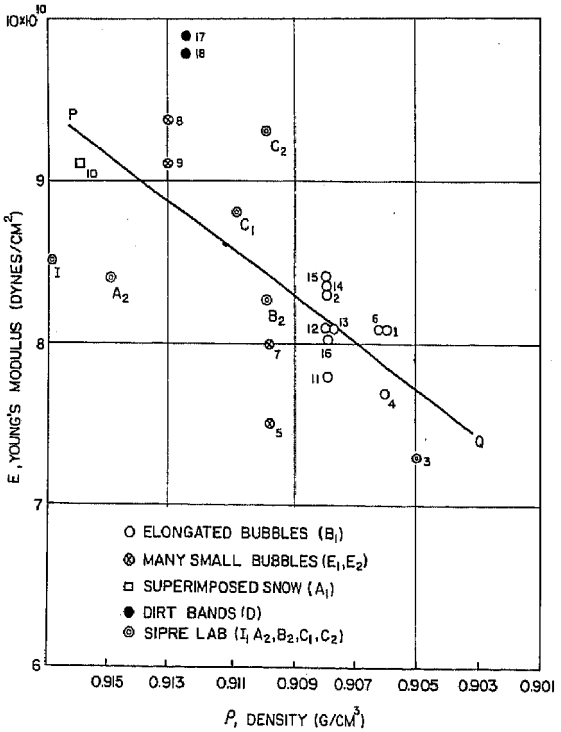

Figure 7. Young's modulus vs density; tunnel ice.

The Young's moduli of these samples are plotted against density in Figure 7. The points are scattered in a wide range, showing that the amount and size of air bubbles affect the elasticity in various ways. In general, however, Young's modulus decreases linearly with the increase of air voids.

The interesting point is that a slight decrease in density results in a rapid decrease in Young's modulus. This is important in the discussion of the relation between Young's modulus and density for the wide range of ice samples taken from the ice cap (Fig. 25). Specimens 5 and 7 in Figure 7, cut from the E1 sample taken horizontally, show much lower values of $\underline{E}$ than specimens 8 and 9 from the vertical E2 sample. The same effect, however, is not observed in the B1 ice. Specimens from one block of B1 ice, which shows a marked orientation of elongated air bubbles, were made with orientation of bubbles in $\underline{x}$, $\underline{y}$, and $\underline{z}$ directions (11 through 16), and no marked anisotropy is observed. The remarkably high value of $\underline{E}$ for the ice containing silt particles shows considerable

promise for the study of frozen soil by this sonic method. The data obtained in the USA SIPRE laboratory are discussed in section 11.

Viscosity measurements were made for six samples. One oscillogram of tunnel ice is reproduced in Figure 29 to show the manner of damping. The mean value of tan δ is 0.0344 for B1 ice, 0.0333 for E1 ice, and 0.0287 for E2 ice. The data show that the mechanical loss is smaller for higher density samples. This point is discussed in section 13.

5. Elastic properties of snow samples from the deep pit

In 1954 a 100-ft deep pit was dug in the ice cap at Site 2, and a series of pegs was fixed to the wall at various depths. These pegs are designated PA, PB, ... PG. PA is located near the surface of the ice cap and PG is at the bottom of the pit. The density of snow near the surface is about 0.45 g/cm^3 and increases to 0.65 at the bottom. Thin sections of samples from various depths were made and the structure was studied under a microscope (Fig. 8-11). The sample from the PB level is ordinary settled snow, but some larger grains are mixed with it (Fig. 8). The grains of snow become larger with depth, and the air space between the grains transforms into a network of air columns. This process can be seen in Figures 10 and 11. In Figure 11, compacted snow at the bottom of the deep pit, the network of air columns is clearly seen. In this stage the snow is still permeable to air, although it looks like translucent solid ice.

The experiments at Site 2 were carried out in a snow laboratory with a temperature kept almost constant at -9C. The walls and ceiling are insulated with glass fiber and the room is cooled by cold air drawn from the deeper levels of the ice cap. Young's modulus was measured in this laboratory and the results are plotted as a function of density (Fig. 12). Most of the data lie on a straight line, except those of PD and PE. These two layers are a little different in structure from the others (Fig. 9) appearing to be compacted granular snow, which would be expected to show a lower Young's modulus than settled snow of the same density. The test results agree with this.

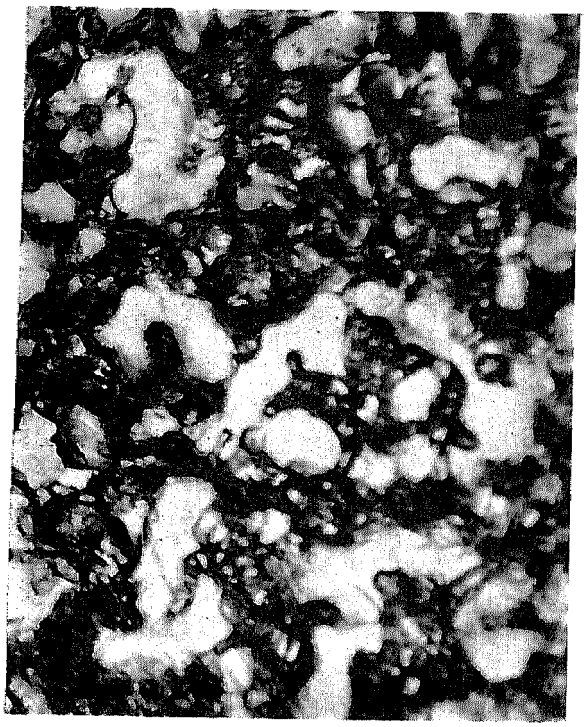

Figure 8. Snow from the deep pit, PB, ρ = 0.49 g/cm^3, x14.

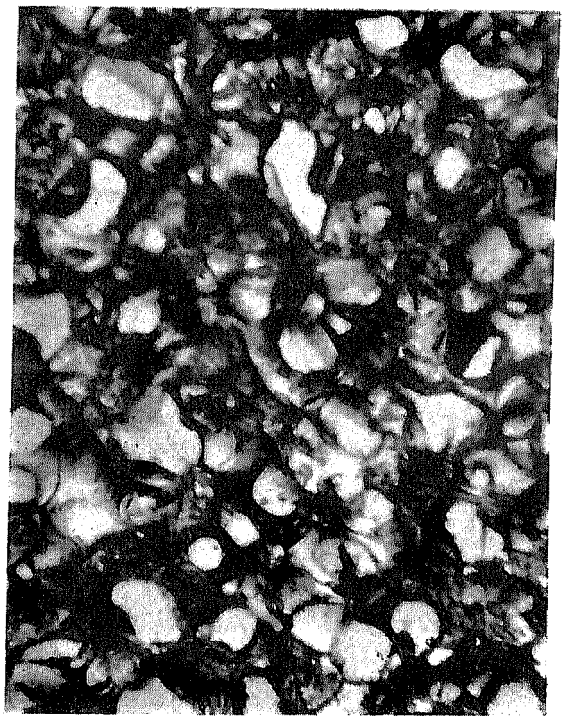

Figure 9. Snow from the deep pit, PD, ρ = 0.57 g/cm^3, x14.

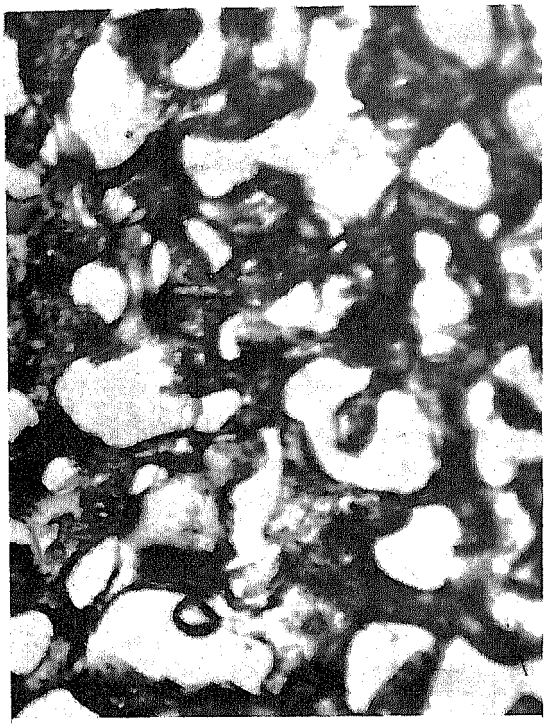

Figure 10. Snow from the deep pit, PF, $\rho = 0.61$ g/cm^3, x14.

Figure 11. Snow from the deep pit, PG, $\rho = 0.64$ g/cm^3, x14.

All the samples mentioned above were taken horizontally from the snow wall with a hand auger. For levels below the bottom of the deep pit, the sample must be taken vertically by drilling. In order to relate the data for deep pit samples to those for core samples, samples taken horizontally and vertically at the same spot of PG were compared (Fig. 13). The results for vertical samples tend to be a little larger, but the difference may be neglected if we are satisfied with the accuracy of 5%. In this series of experiments the length of the bar was also varied between 24.9 cm and 14.9 cm, and the thickness between 5.5 mm and 9.9 mm, so that the resonance frequency varied

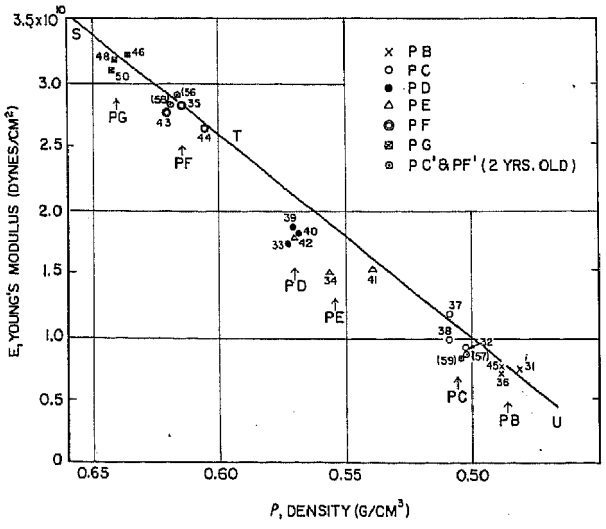

Figure 12. Young's modulus vs density; PC' and PF' are 2 yr old. Tests at -9C.

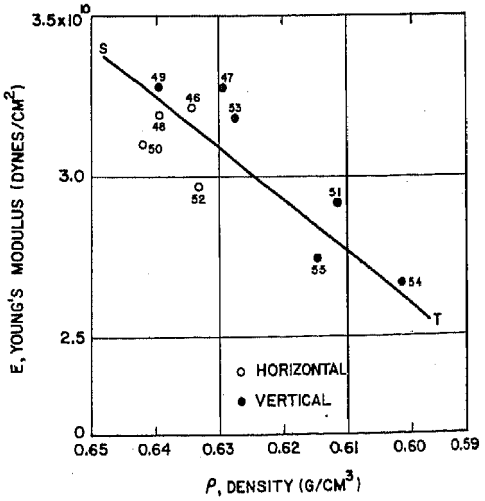

Figure 13. Comparison of the samples taken horizontally and vertically at PG, f = 210 - 575 cps. ST = ST (Fig.12).

between 210 and 575 cps. Young's modulus is a function of frequency, and it decreases slightly with the frequency, as described in section 11. Figure 13 can be interpreted to show that the effect of frequency also may be neglected if an accuracy of ± 5% is sufficient.

The snow deep in the ice cap is subjected to an intense stress, which is released when the sample is removed from the wall. The elastic nature might be different for a new sample and an old sample taken from the same level. At the levels of PC and PF in the deep pit, core samples were taken two years ago and left in the core holes until this year. These samples were tested in the same way as the new samples, and the data are plotted in Figure 12 as PC' and PF'. These points lie on the same line, and it is seen that the release of internal stress does not affect the Young's modulus appreciably.

6. Elastic properties of core samples obtained by drilling

Drilling in the ice cap was carried out in 1956 and 1957, and 4-in. core was obtained from various depths. When drilling goes deeper than about 60 m, the ice becomes impermeable to air and the network of air columns seen in Figure 11 transforms into a group of air columns and bubbles (Fig. 14). In a long period of time the air column splits into a series of air bubbles because of the effect of surface energy (Fig. 15). The mechanism of this transformation has been described in detail for vacuum figures of columnar shape in single crystals of ice (Nakaya, 1956). The mechanism is the same for both cases, the only difference being that the process is much slower in the case of air columns. Still deeper, the air bubbles become smaller and smaller as the ice is compacted because of its viscous nature. The pressure of the bubble becomes higher and higher. Langway (personal communication) measured a mean value of pressure as high as 26 atm. Ice from the deep layers of the ice cap is a peculiar material containing numerous infinitesimal air bubbles of high pressure.

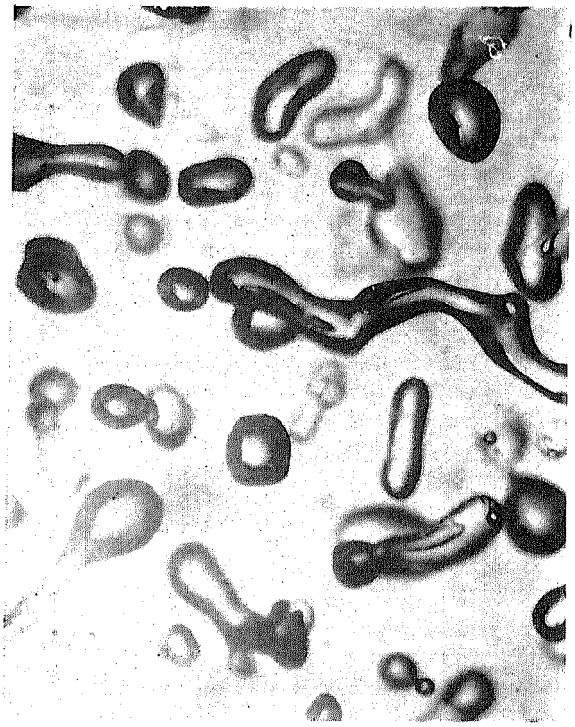

Figure 14. 1956 core from 84 m depth. $\rho = 0.880$ g/cm³, x 14.

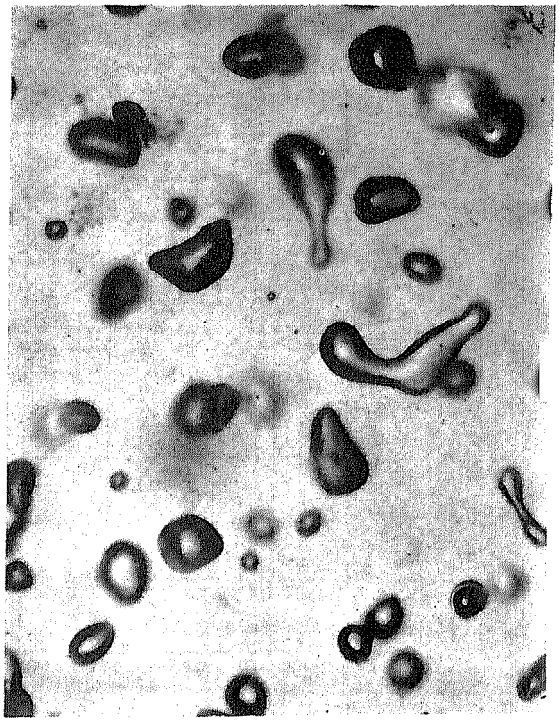

Figure 15. 1956 core from 113 m depth. $\rho = 0.899$ g/cm³, x 14.

The Young's modulus of 1956 and 1957 cores was measured and plotted as a function of density (Fig. 16). The core samples of density below 0.65 g/cm^3 give values corresponding to those obtained for the deep-pit samples. The most interesting point is that all data obtained for the deeper layers lie on a straight line RS which is an extension of SU. Young's modulus is a linear function of the density for this wide range. The empirical equation of this line is

$$E = (16.4\,\rho - 7.20) \times 10^{10} \qquad (16)$$

for the range of ρ between 0.9 and 0.5 g/cm^3.

Young's modulus for pure ice is nearly 9×10^{10} dynes/cm^2, and the extension of this line to $\rho = 0.917$ gives a much lower value. This point agrees with the phenomenon shown in Figure 7; the rapid decrease in Young's modulus with the slight decrease in density. The $\underline{E}$-ρ relations from Figure 7 and Figure 16 are shown together in Figure 17. There appears to be a discontinuity in the slope at X, in Figure 17, at the density of about 0.905 g/cm^3. It is difficult to figure a mechanism which gives a discontinuity in the elasticity at such a density. The transition from PQ to RS may take the course shown by Y in Figure 17. In any case the experimental results show that Young's modulus decreases very rapidly when the density deviates slightly from that of pure ice and after $\rho = 0.905$ the rate of decrease diminishes markedly.

There is another possible interpretation of this phenomenon. The nature of tunnel ice may be qualitatively different from that of deep core samples. The deepest layer from which a sample was taken was 155 m from the surface. This ice may be about 300 or 350 years old but not much older. The tunnel ice, however, may be very much older, if the ice near the bottom of the ice cap flows towards the edge of the ice cap. In that case, the elastic nature may be different for these two types of ice.

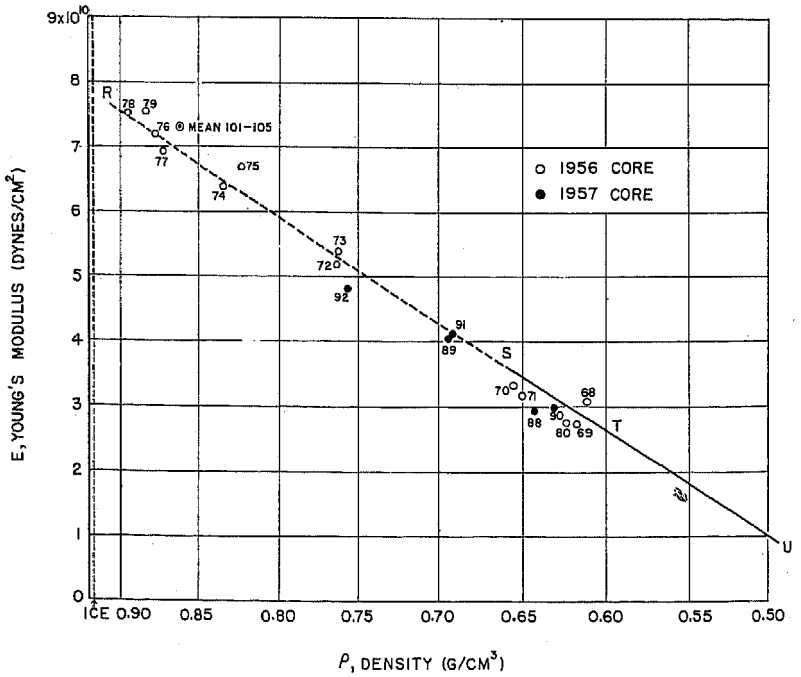

Figure 16. Young's modulus vs density; 1956 and 1957 core. Line SU corresponds to SU in Figure 12.

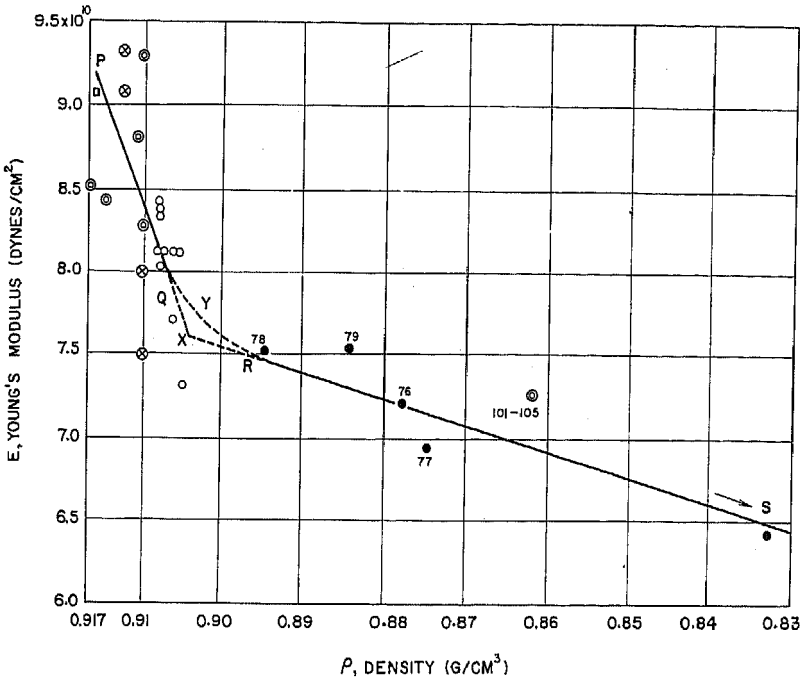

Figure 17. Young's modulus vs density, tunnel ice and core samples. Lines PQ = tunnel ice (from Fig. 7), RS = core samples (from Fig. 16).

7. Elastic properties of snow near the ice-cap surface

Vertical variation of Young's modulus near the surface. In 1956 a large trench was made at Site 2 in order to set up a drill rig. The snow wall of this trench has been exposed to the atmosphere for a year, and the surface was etched so that the layer structure of snow cover was faintly visible. A block of snow about 1 m in thickness was cut from this wall and sliced horizontally into 18 sheets. Young's modulus and density were measured for each of these slices and the vertical distribution was examined (Fig. 18). The density and Young's modulus show a good parallelism; both values show a minimum in the coarse-grained layer and a maximum in the icy layer.

The relation between Young's modulus and density is shown in Figure 19, irrespective of the nature of snow. The points are scattered in a wide range, although the general tendency is toward a linear relationship between E and ρ. ΔE/E is about 30% when all types of snow are treated as a whole. For the ordinary

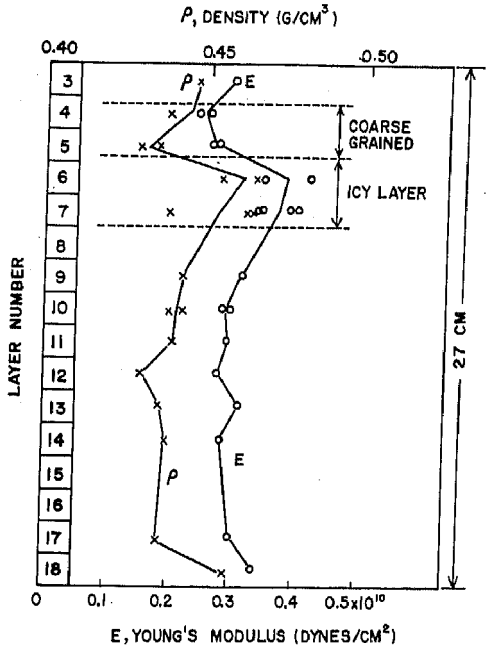

Figure 18. Vertical distribution of Young's modulus (at -9C) and density, snow near the surface; samples 3-22.

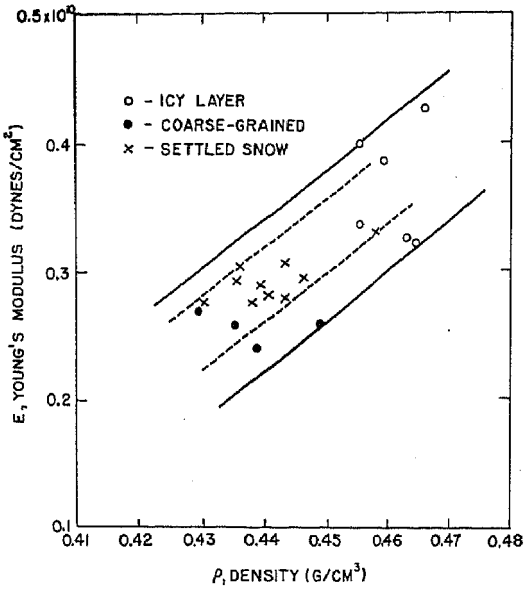

Figure 19. Young's modulus (at -9C) vs density, snow near the surface; samples 3-22.

settled snow only, $\Delta E/E$ reduces to nearly 15%. Young's modulus for snow is considered to be a function of density and structure of snow. As the slow natural densification of snow proceeds, Young's modulus becomes larger than for ordinary settled snow of the same density. When snow becomes granular, the reverse will be the case. This point is discussed in detail later (see Fig. 23, 24).

Wind-packed snow. The snow on the surface of the ice cap is sometimes packed by the wind. Wind-packed snow shows a slight increase in density, but the hardness value becomes very large. The structure of new wind-packed snow is shown in Figure 20. Some of the snow particles undergo metamorphism, while others still show the original shape of snow crystals. These particles are bonded together, which causes an increase in Young's modulus.

Peter snow. The snow disaggregated and deposited by the Peter snow miller, called "Peter snow", has a high density and becomes quite hard within a few weeks. In the summer of 1956 an accumulation of Peter snow about 1 m in thickness was made and

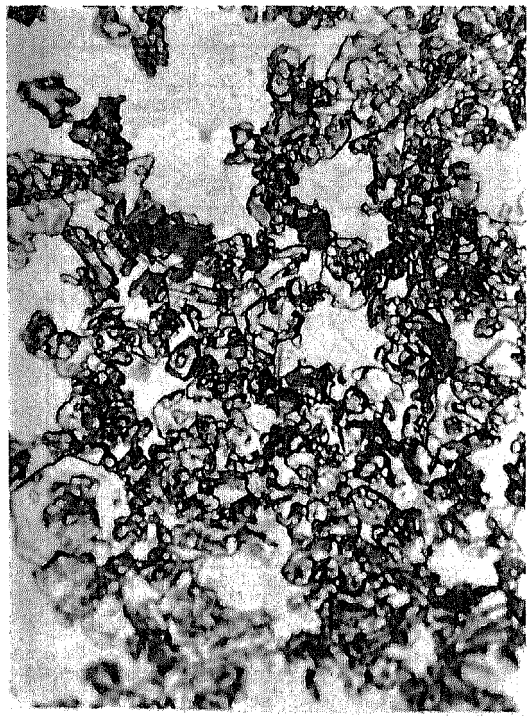

Figure 20. Wind-packed snow, $\rho = 0.35$ g/cm³, x14.

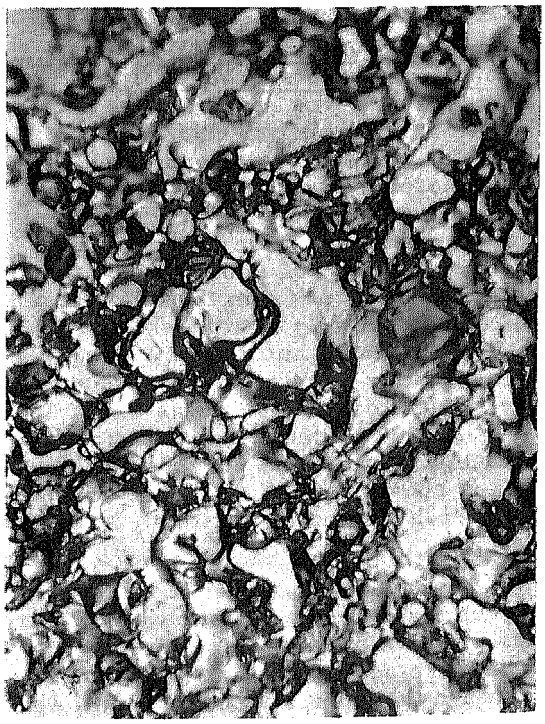

Figure 21. Peter snow, 1-yr old, $\rho = 0.53$ g/cm³, x14.

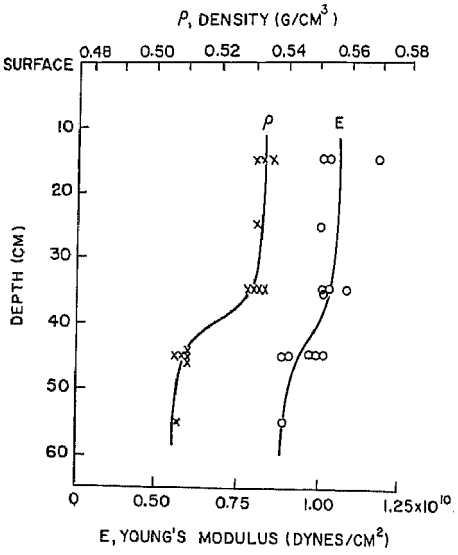

left for a year. Blocks were cut from this accumulation, and the vertical distribution of Young's modulus and density were studied (Fig. 22). Both Young's modulus and density are higher than corresponding values for the sample from PC in the deep pit. They are almost constant to the depth of 40 cm from the surface and become smaller below 40 cm. The structure of Peter snow is shown in Figure 21. It is interesting to note that the structure is similar to that of the sample taken from the deep pit.

Figure 22. Vertical distribution of E (at -9C) and ρ in 1-yr old Peter snow; samples 23-30, 81-86.

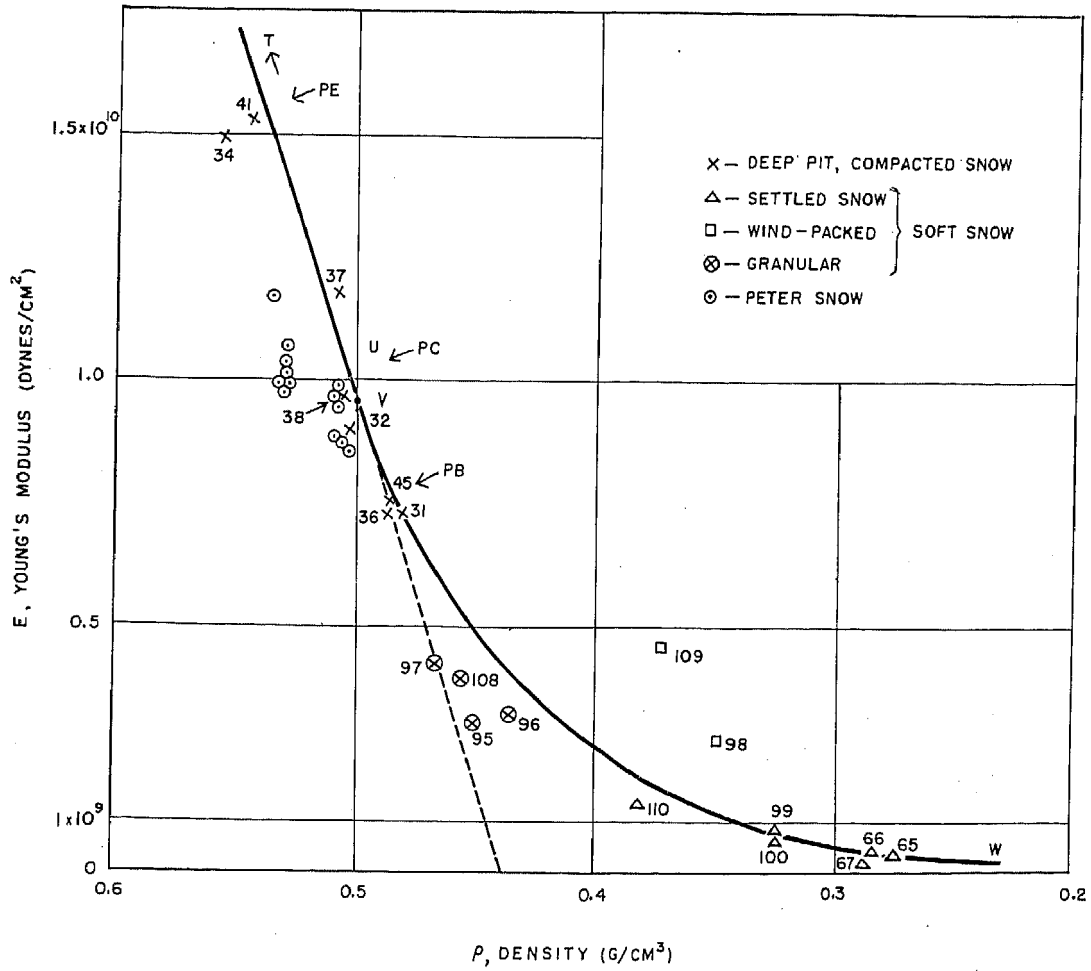

Figure 23. Young's modulus (at -9C) vs density, snow near the ice-cap surface. TU represents the data for deep-pit samples; VW is the exponential curve for settled snow.

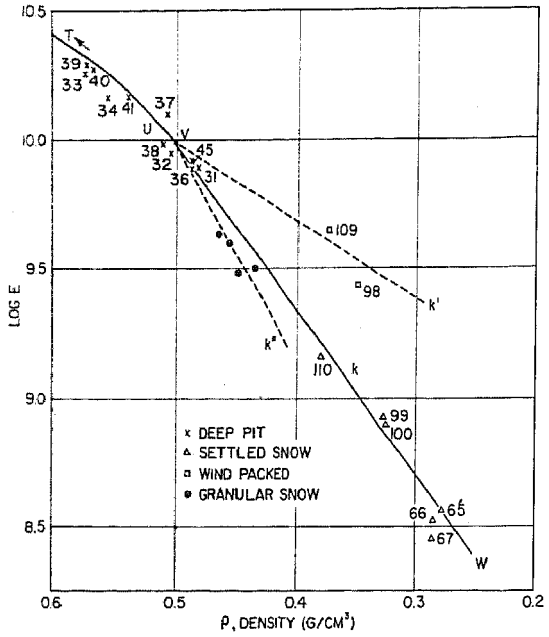

Figure 24. log E vs ρ, snow near the ice-cap surface.

Relation between Young's modulus and density of snow. Figure 23 shows Young's modulus vs density for ordinary settled snow, wind-packed snow, granular snow, and Peter snow. The interesting point is that the data for wind-packed snow are decidedly higher than the line for ordinary settled snow (VW). Young's modulus of wind-packed snow is usually a few times larger than that of settled snow of the same density. For granular snow, the contrary is the case. Young's modulus is not only the function of density, but it must be influenced by the bonding of particles and possibly by the size distribution. The present result agrees with this concept.

To get a closer insight, the data are plotted on a semilogarithmic scale (Fig. 24). The exponential portion is expressed by the straight line VW. The empirical equation takes the form

$$E = C \exp\left(-k(0.50-\rho)\right) \qquad (17)$$

for the range of ρ between 0.50 and 0.25 g/cm³. k is a factor determined by the structure of the snow, and may be called the "structure factor". The structure factor increases as bonding between particles becomes stronger. In Figure 24, the structure factor for wind-packed snow is k' and for granular snow k''. For ordinary settled snow k is 6.35 and the empirical formula is

$$\log E = 6.80 + 6.35\rho. \qquad (18)$$

Up to this stage the structure factor is only a mathematical expression. It is desirable to correlate this factor with the configuration of snow particles by experiments. For that purpose examination of the structure of snow by Fuchs's method (1956) must be carried out in parallel with the sonic experiments. Once the relation between k and snow structure is established, this structure factor may be introduced effectively into snow mechanics.

The data for Peter snow (Fig. 23) are close to the data for PC in the deep pit. The so-called powder snow observable in the Greenland Ice Cap is difficult to compact artificially, but over a long period of time it becomes compacted by the weight of overlying snow deposits. In a few weeks or months Peter snow reaches the compacted state which corresponds to that at PC in the deep pit. The natural compaction at PC required about 20 years, so that the process of making Peter snow may be considered to shorten the time of 20 years to a few weeks or a few months.

8. Relation between Young's modulus and density over the range from surface snow to ice

Combining Figures 7, 12, 16, and 23, the relation between Young's modulus and density is plotted for the whole range of snow and ice observable in the Greenland Ice Cap (Fig. 25). The whole range is divided into three regions, I, II, and III. When the density deviates slightly from pure ice, Young's modulus decreases rapidly. This is region I, called the ice region for descriptive purposes. The samples of this region were obtained from the ice tunnel. The range of density is between 0.917 and 0.90 g/cm³. The material is almost ice with small air voids.

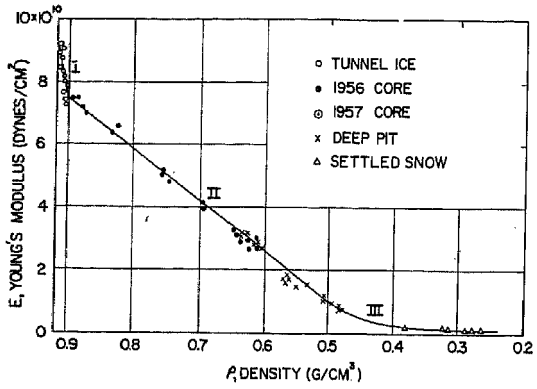

Figure 25. Young's modulus vs density for the whole range of Greenland snow and ice.

Region II covers the range of density between 0.90 and 0.50 g/cm³. The samples from the wall of the deep pit and the core samples obtained by drilling are in this region. The material is in the intermediate state between snow and ice, and its general appearance is that of translucent ice. Most of the samples in this region, however, are still permeable to air. This region is called the core region. It is noteworthy that the relation between Young's modulus and density is expressed by a straight line for the whole range of this core region.

Region III is the soft snow near the surface of ice cap, density between 0.50 and about 0.25 g/cm³. This is called the snow region. The samples in this region show a variety in nature. For ordinary settled snow, Young's modulus decreases in an exponential form with decrease in density. The data for wind-packed snow lie above this exponential curve, and those for granular snow below this curve. The physical interpretation of this E - ρ relation for the whole range of ice and snow is one of the important problems on the nature of the Greenland Ice Cap.

9. Supplementary experiments on the elastic nature of snow and ice at Site 2

Anisotropy of Peter snow. Two sets of rectangular bars were made from 1-yr old Peter snow with the width of the bar corresponding to the horizontal plane (H), and the vertical plane (V). If there is any anisotropy in the structure of Peter snow, the Young's modulus should be different for H and V samples. For example, if Peter snow has a horizontal layer structure, V samples should show a higher Young's modulus than H samples, as sliding between sublayers of H is considered to facilitate bending (Fig. 26b). The difference is not marked (Fig. 26a), but V is clearly higher than H, showing that Peter snow has a trace of horizontal layer structure.

Age hardening. A preliminary experiment on age hardening was carried out on new soft snow and 1-day old Peter snow. Two samples of new soft snow (No. 66, 67, Fig. 27) were kept in the laboratory at -9C after measuring Young's modulus. Young's modulus increased to nearly twice its initial value in one day and then the curve followed the saturation type (Fig. 27).

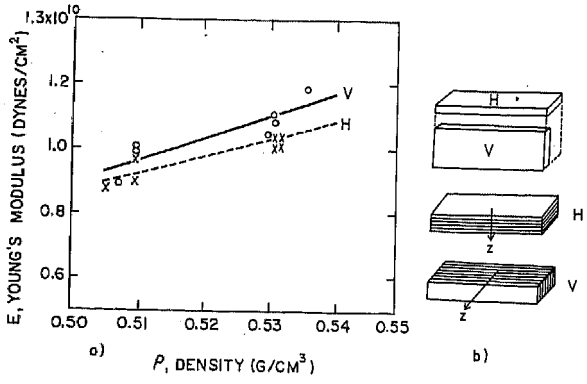

Figure 26. Anisotropy of 1-yr old Peter snow; samples 23-30, 81-86.
H = Width corresponds to horizontal plane.
V = Width corresponds to vertical plane.

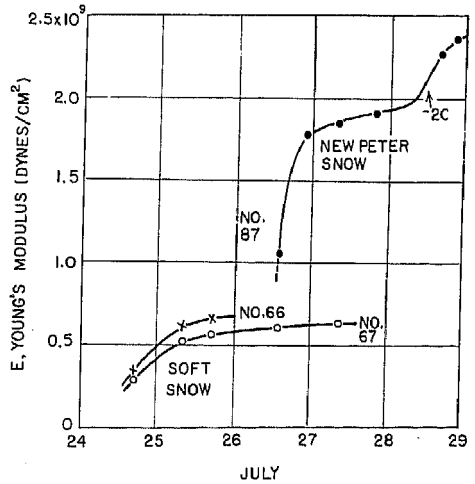

Figure 27. Age hardening of soft snow and Peter snow. At -9C except for a few hours at -2C on 28 July.

A similar experiment was carried out with 1-day old Peter snow. The rapid increase of Young's modulus is remarkable. This rapid hardening phenomenon is almost completed in half a day or so, and then the curve follows the saturation type. During the morning of 28 July, the room temperature accidentally rose to -2C for a few hours and then cooled down to -9C. This caused a second jump in the Young's modulus (Fig. 27). These experiments are of preliminary nature, but the result shows that this sonic method is very useful in the study of the mechanism of age hardening of snow.

Temperature dependence of Young's modulus of core ice. The temperature dependence of Young's modulus was studied for two samples of 1957 core; from 26 m and 61 m depths (Fig. 28). Although the temperature range is limited, -2C to -9C, the increase in Young's modulus with decrease of temperature is confirmed. A similar experiment on the tunnel ice (section 11) showed a less marked temperature dependence. This point must be studied in more detail in future experiments.

10. Viscosity measurement of snow and ice in Greenland

Viscosity measurements were carried out by the damping method for various samples of snow and ice from the ice cap. Damping was fairly rapid at -5C or -9C temperatures. Four examples of oscillograms are shown in Figures 29-32. The value of tan δ was calculated by eq 13. The loss factor for new soft snow (Fig. 30) is 0.361, the maximum value among all samples tested. The deposited coarse-grained snow has a lower tan δ, 0.0905 for sample A1 (Fig. 31). As the density increases still further, tan δ becomes 0.049 for the core sample of density 0.757 g/cm^3 (Fig. 32) and 0.0332 for tunnel ice B1 (Fig. 29), density 0.908 g/cm^3. There appears to be a simple relation between density and the loss factor, but the frequency dependence is not negligible so that no conclusion can be drawn unless the frequency correction is made. This point is discussed in detail in section 12.

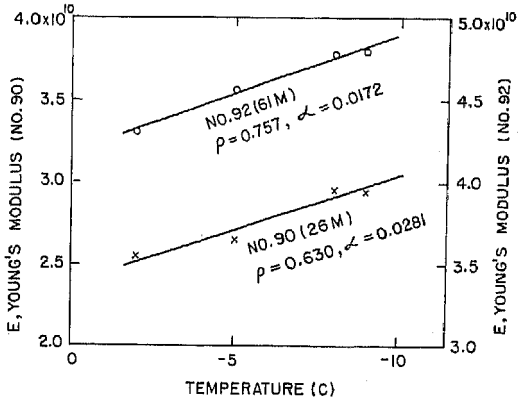

Figure 28. Temperature dependence of Young's modulus; 1957 core.

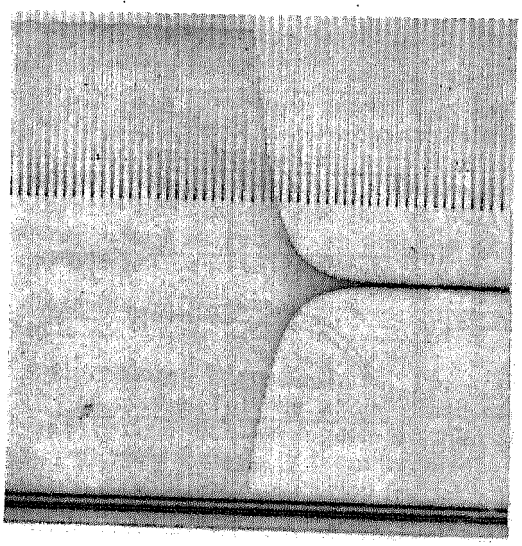

Figure 29. Oscillogram of tunnel ice T2. ρ = 0.908, f = 254, E = 8.3 x 10^{10}, tan δ = 0.0332, temp -5C.

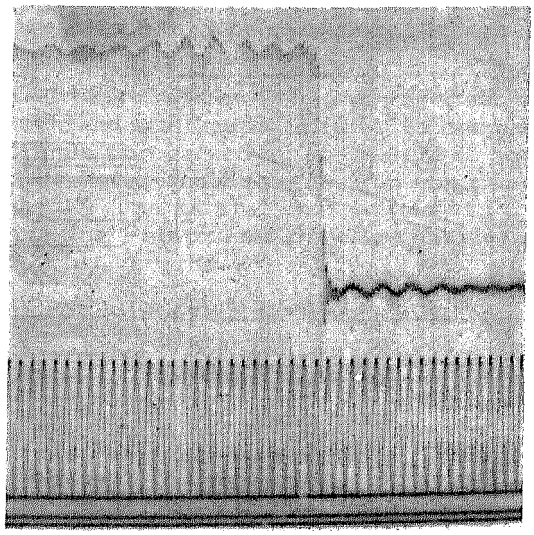

Figure 30. Oscillogram of new soft snow, no. 67. ρ = 0.288, f = 105, E = 0.028 x 10^{10}, tan δ = 0.361, temp -9C.

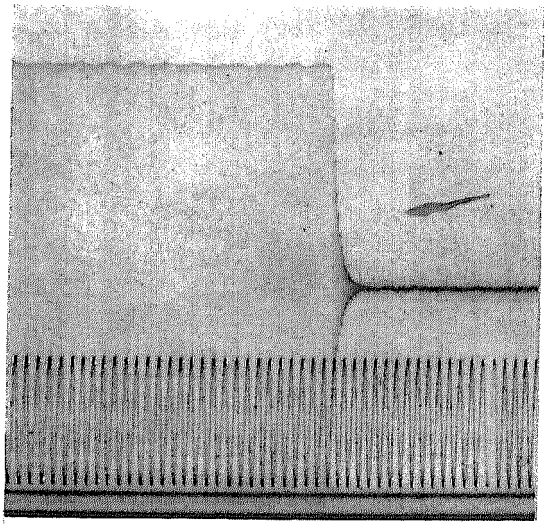

Figure 31. Oscillogram of coarse-grained snow, no. 41. $\rho = 0.538$, $f = 281$, $E = 1.53 \times 10^{10}$, tan = 0.0905, temp -9C.

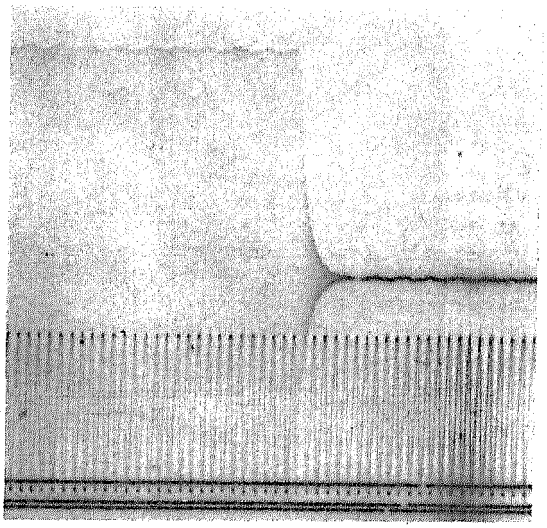

Figure 32. Oscillogram of 1957 core, no. 92. 61 m depth, $\rho = 0.757$, $f = 360$, $E = 4.78 \times 10^{10}$, $\tan \delta = 0.049$, temp -9C.

There is another method of determining $\tan \delta$. From visco-elastic theory:

$$\tan \delta = \frac{1}{\sqrt{3}} \frac{\Delta f}{f_{max}} \qquad (19)$$

where f_{max} is the resonance frequency, and Δf is the difference, measured from the resonance curve, of the frequencies at which the amplitude becomes one-half of the maximum amplitude. (The meaning of f_{max} and Δf is clear from Figure 34).

The resonance curve is obtained from an oscillogram made by changing the frequency of the exciting current successively. An example is shown in Figure 33. For this oscillogram the exciting frequency was changed by 10-cycle intervals, starting from $f = 270$ cps. The maximum amplitude is observed at $f = 350$ cps. The amplitude is measured at each frequency and plotted (Fig. 34). Similar measurement was made for samples 90 and 92. It is noted that the resonance curve shows bilateral symmetry for sample 90, but not in the other cases. For 90, the value of $\tan \delta$ calculated from the damping is 0.074, and the value obtained from the resonance curve is 0.071. In this case the agreement is satisfactory. For samples 49 and 92, the calculated values are 0.0606 and 0.049 respectively, while the corresponding values obtained from the resonance curve are 0.078 and 0.064. The difference is much larger than the experimental error. The results of these experiments show that the resonance curve method may be applied when the curve is symmetrical but not when it is unsymmetrical.

The values of $\tan \delta$ obtained for various samples of snow and ice in Greenland were studied in detail, but it was difficult to find some relations. For example, $\tan \delta$ shows no simple relation to density. It was found that the frequency dependence plays an important role in this case and no simple relation to density is obtained when frequency varies for different measurements. The resonance frequency is very sensitive to the size of sample, and it is difficult to carry on the measurement with a fixed value of frequency. In the case of core samples, the frequency varied between 291 and 650 cps, because a long enough sample could not be obtained for the deep cores.

In Figure 35, $\tan \delta$ is plotted as the function of frequency, irrespective of the density. Each group is expressed as a decreasing function of frequency, and all the curves show more or less similar behavior. This means that the frequency dependence must be taken into account in treating the viscous nature of ice or snow.

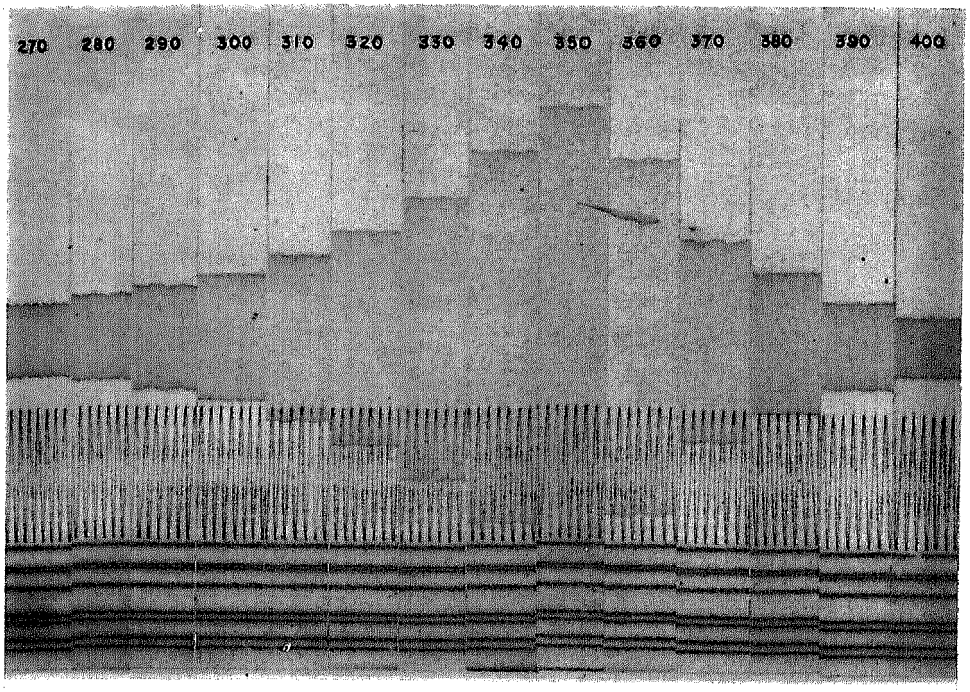

Figure 33. Oscillogram of sample 49 from deep pit PG. $\rho = 0.640$, $E = 3.28 \times 10^{10}$, $\tan\delta = 0.0606$. f is changed by 10 cycle intervals starting from 270 cps.

11. Further experiments on the elastic nature of tunnel ice

Four samples of tunnel ice (Table II) were brought back to the USA SIPRE laboratory and their elastic and viscous behavior was investigated as a function of temperature and frequency.

Temperature dependence of Young's modulus. Young's modulus increases slightly as the temperature decreases and a hysteresis phenomenon is observed. Starting from -5C, the temperature was lowered to -30C. The sample was left overnight at -30C, but not much change was observed in the Young's modulus. The samples were warmed up to -22C and left overnight. The Young's modulus was almost the same as that observed at -30C, showing a marked hysteresis phenomenon. When the samples were warmed up to -10C, the increase in Young's modulus was about 5% of the former value, except for the commercial ice. The nature is similar to the case of hardening of metals by quenching. The results are shown in Figure 36. This hysteresis phenomenon is important for clarifying the elastic nature of this peculiar type of ice.

Taking the mean of the hysteresis curve, the relation between Young's modulus and temperature is shown in Figure 37 for four samples of tunnel ice and two samples of commercial ice. For most of them, E shows a tendency to increase linearly with decrease of temperature, but the rate of increase is slightly larger above -10C than below -10C. Assuming the linear relation

$$\frac{\Delta E}{E} = -\alpha\theta$$

the coefficient α is calculated for the range above -10C. Corresponding values are obtained for core samples (Fig. 28). Summarizing the results:

$\rho = 0.630$, $\alpha = 0.0281$; core from 26-m depth

$\rho = 0.757$, $\alpha = 0.0172$; core from 61-m depth

$\rho = 0.910$, $\alpha = 0.0026$; tunnel ice B, C.

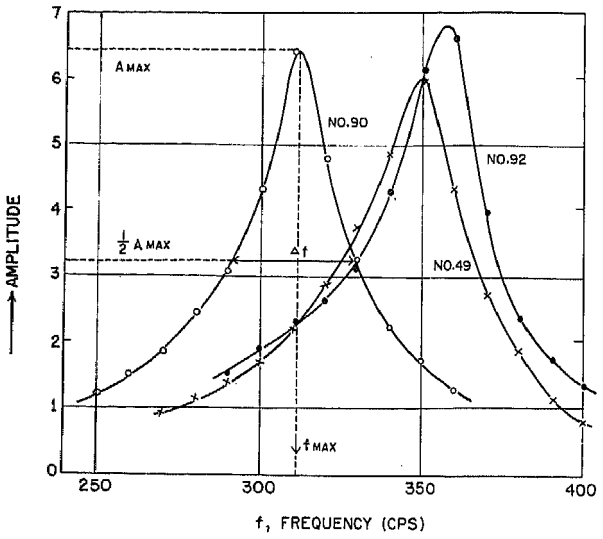

Figure 34. The resonance curve; amplitude versus frequency.

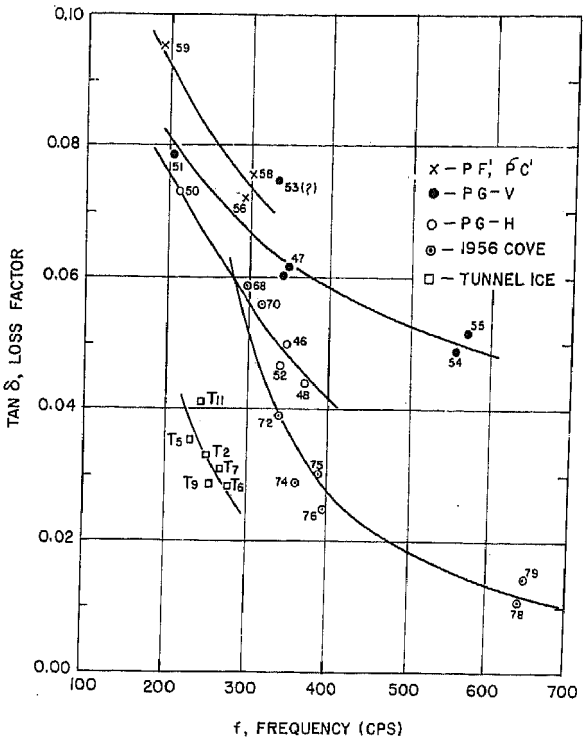

Figure 35. Frequency dependence of loss factor.

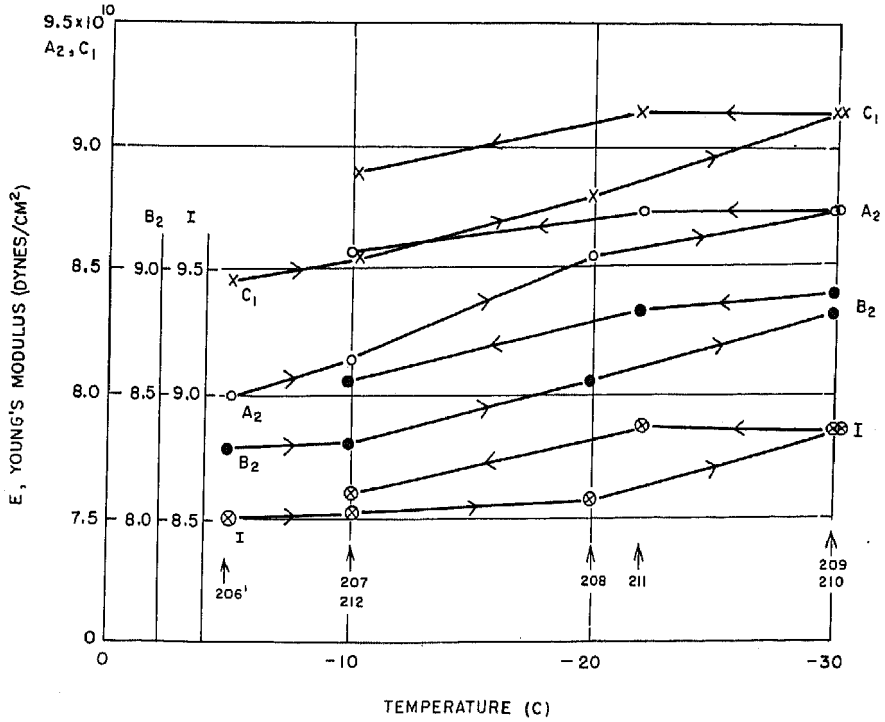

Figure 36. Hysteresis phenomenon in the relation between Young's modulus and temperature. Arrows and nos 206'-212 show sequence of measurements.

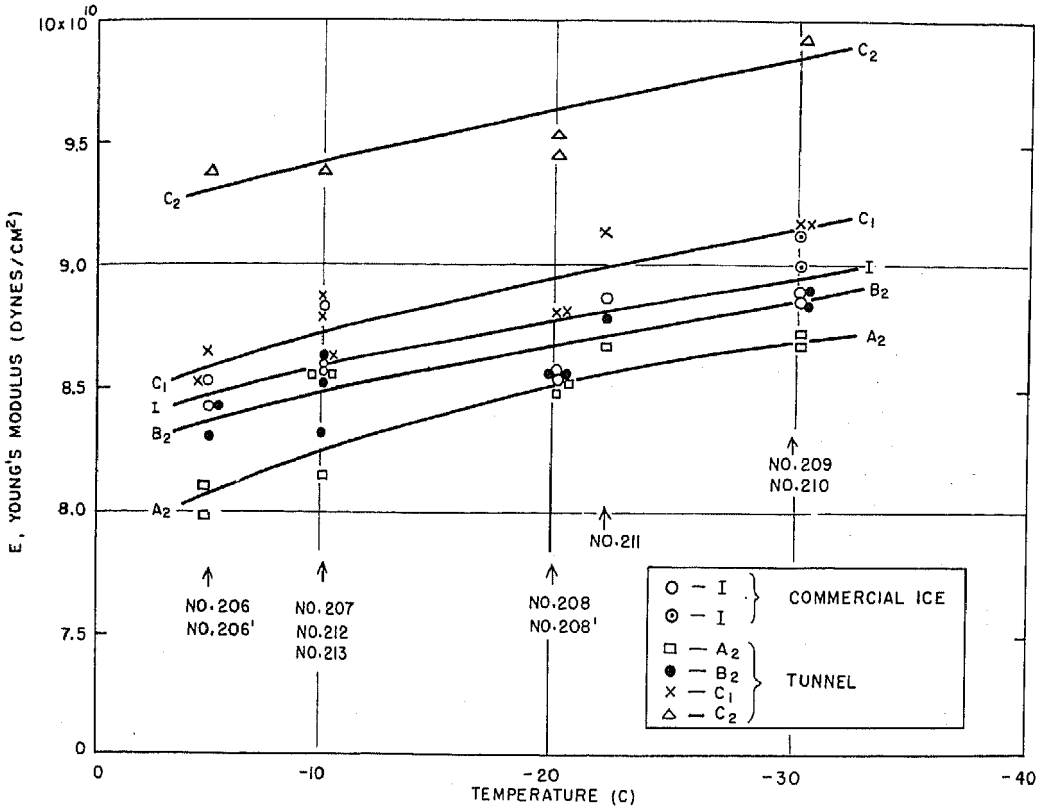

Figure 37. Young's modulus vs temperature.
(Taking the mean of the hysteresis curve, see Fig. 36.)

The temperature coefficient decreases with increase in density. In other words, temperature dependence is more marked for compacted snow than ice. For the tunnel ice the coefficient decreases to 0.0021 below -10C.

Frequency dependence of Young's modulus. In order to study the effect of frequency on Young's modulus, the sample was shortened successively, and Young's modulus was measured at each stage of shortening of the sample. By this method Young's modulus could be measured as the function of frequency with respect to one sample. This is an advantage, but there is a disadvantage also. The hysteresis effect, if it exists, cannot be studied by this method.

After the experiments shown in Figure 36, four samples of I, A2, B2, and C1 ice were made with the same dimensions; ℓ = 309.0 mm, $\underline{b}$ = 20.0 mm, $\underline{h}$ = 6.4 mm. This size gives a frequency of about 200 cycles. The samples were shortened in four stages to the length of 185.1 mm, corresponding to a frequency of about 580 cycles. Young's modulus was measured at each stage and the frequency dependence was obtained (Fig. 38). For all samples tested, Young's modulus tended to decrease with increase in frequency and approach a constant value in the higher frequency range. However, the curves cannot be taken to show the frequency dependence of Young's modulus without considering the hysteresis phenomena of temperature dependence. After finishing the experiments at the length of 185 mm (no. 217 in Fig. 38) the samples were left overnight at -10C, and the same measurements were repeated. The value of Young's modulus (no. 217') came back more or less near to the initial value at low frequency. This shows that some phenomenon similar to fatigue must be mixed with the effect of frequency. In fact, in the other series of experiments, Young's modulus was sometimes constant or nearly constant for the whole range of frequency, 140 cycles through 600 cycles (two series of experiments for A2 ice in Fig. 39).

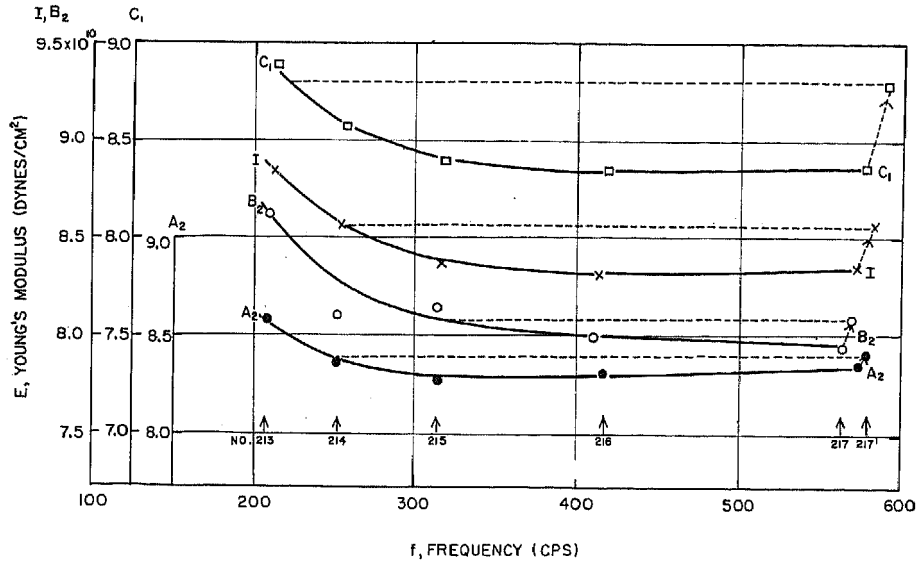

Figure 38. Frequency dependence of Young's modulus. Temp -10C, nos. 212-217' show sequence of measurements.

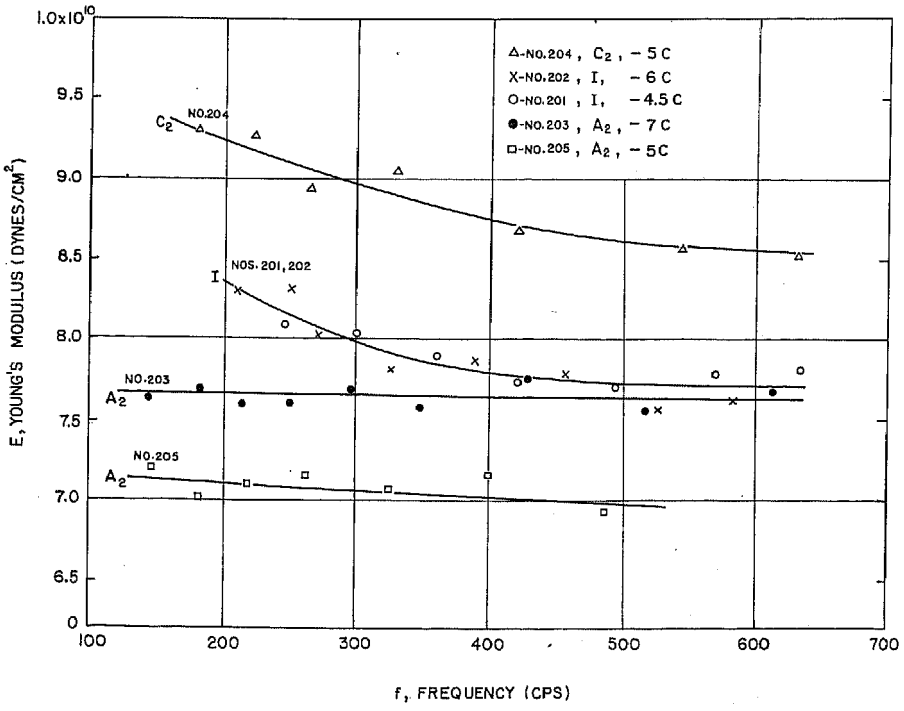

Figure 39. Frequency dependence of Young's modulus; -4.5C — -7C, nos. 201-205.

However, the data for the commercial ice and C2 ice show a tendency similar to that of Figure 38. It appears that the ice samples from the Greenland Ice Cap have such a variety of elastic natures that any hasty conclusion would be undesirable. In any case the effect of frequency is not so intensive in the case of Young's modulus, and the frequency effect may be neglected if 10% error is admitted in the discussion of the results. The frequency dependence is a powerful tool for the physical investigation of the visco-elastic properties of ice, and further investigations should be carried out in this line.

12. Further experiments on the viscous nature of tunnel ice

Temperature dependence of loss factor. The effect of temperature is most conspicuous in the sample of C2 ice (Fig. 40-43). Figure 40 shows the damping of C1 ice because no data are available for C2 ice at -5C. The difference between C1 and C2 is negligible at this temperature, although it is appreciable at temperatures below -20C. As seen from the oscillograms, the rate of damping decreases remarkably with lower temperature. The loss factor at -30C is only $1/35$ of that at -5C. This means that the activation energy is fairly large for C2 ice. The temperature dependence was studied in the range of -5C and -30C (Fig. 44). A hysteresis phenomenon similar to that for Young's modulus was observed. When the sample was cooled down to -30C, the loss factor decreased remarkably, showing that the energy loss due to internal friction diminishes rapidly with decrease in temperature. Then the sample was warmed up to -10C, and $\tan\delta$ showed a smaller value than the former value at -10C. As $\tan\delta$ is a measure of non-elastic nature of the material, this hysteresis behavior corresponds to the increase in Young's modulus by the same process (Fig. 36).

In order to correlate the loss factor to the internal viscosity, it is necessary to adopt some model. As the first approximation, two well known simple models will be considered, the Voigt model and Maxwell model. According to eq 14, the coefficient of viscosity is proportional to $\tan\delta$ for the Voigt model, and inversely proportional for the Maxwell model. The ordinary viscosity, η, must increase with decrease in temperature. In this meaning the Maxwell model is adopted for this case. Yosida (1956) used the Maxwell model in his study of deposited snow for the same reason, and succeeded in developing his theory of the mechanics of snow. Adopting the Maxwell model, the viscosity coefficient η is calculated by

$$\eta = \frac{E}{\omega \tan\delta} \,. \qquad (20)$$

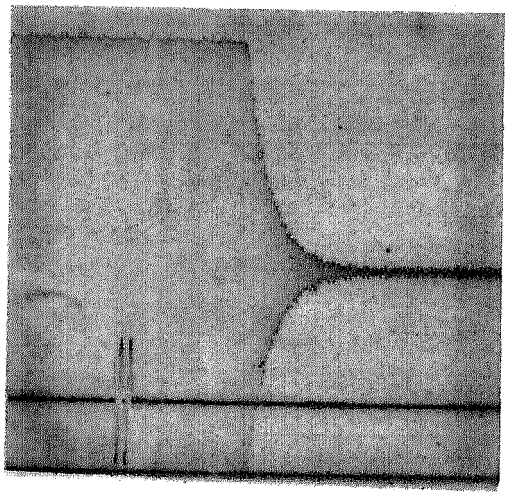

Figure 40. Oscillogram of C1 ice, no. 206, temp -5C. $\rho = 0.911$, $E = 8.47 \times 10^{10}$, $\tan\delta = 0.0345$.

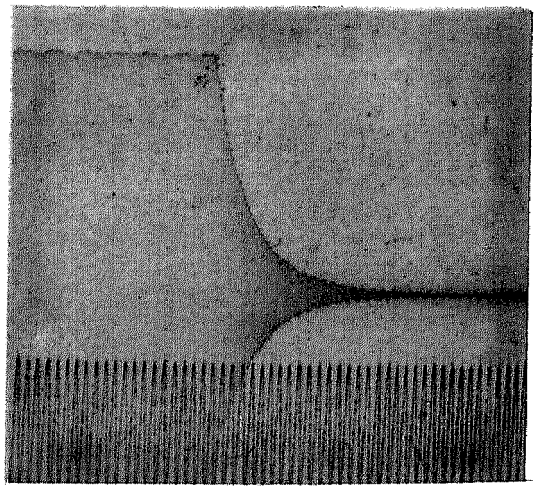

Figure 41. Oscillogram of C2 ice, no. 207, temp -10C. $\rho = 0.910$, $E = 9.39 \times 10^{10}$, $\tan\delta = 0.0206$.

GPO 820866-5

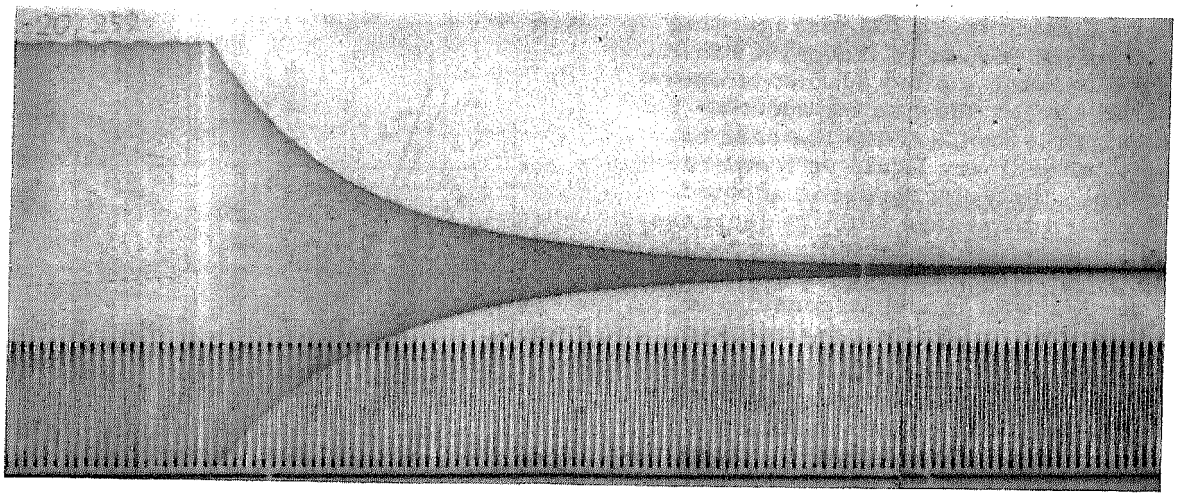

Figure 42. Oscillogram of C2 ice, no. 208, temp -20C.
$\rho = 0.910$, $E = 9.52 \times 10^{10}$, $\tan \delta = 0.0049$.

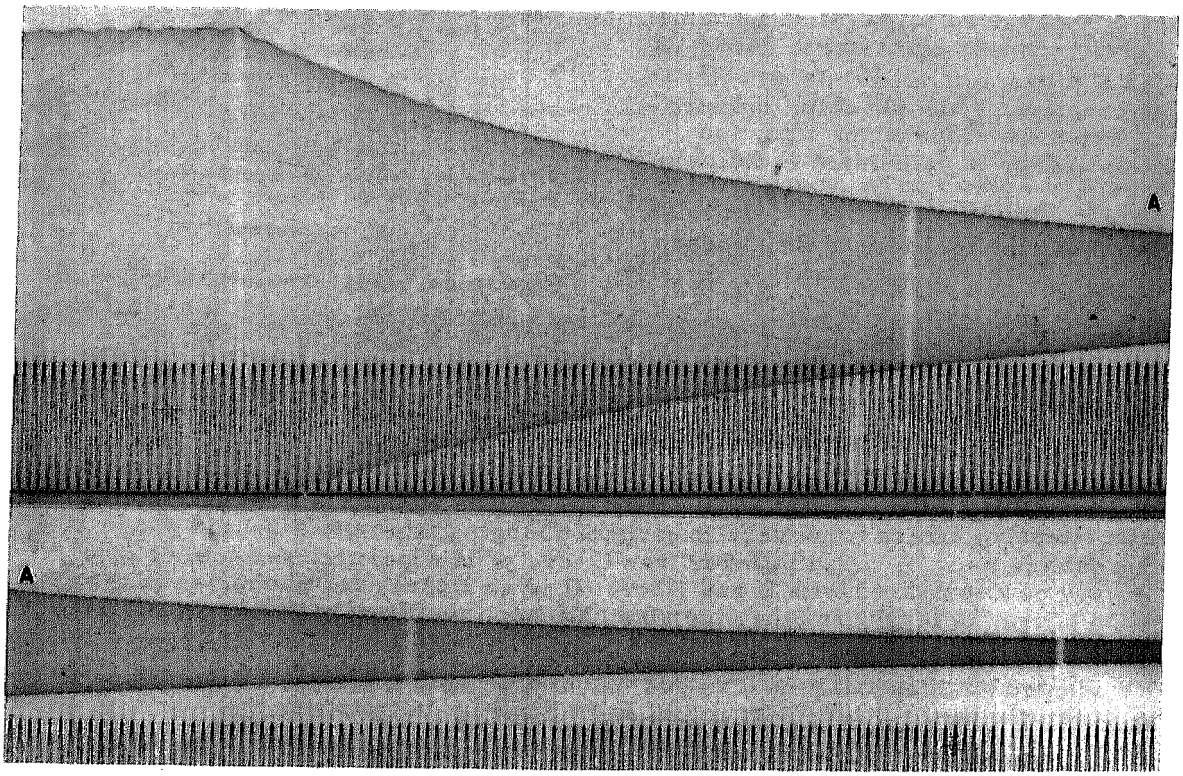

Figure 43. Oscillogram of C2 ice, no. 209, temp -30C.
$\rho = 0.910$, $E = 9.91 \times 10^{10}$, $\tan \delta = 0.0012$.

If η is calculated by eq 20, disregarding the hysteresis portion of the curves in Figure 44, and is plotted against temperature, all curves show an exponential form, which is familiar for the case of viscosity of ordinary liquid vs temperature. When the Voigt model is adopted, the viscosity decreases with the decrease in temperature, which is contrary to the ordinary conception of viscosity. Therefore, the Maxwell model is considered to be a good choice in the present case.

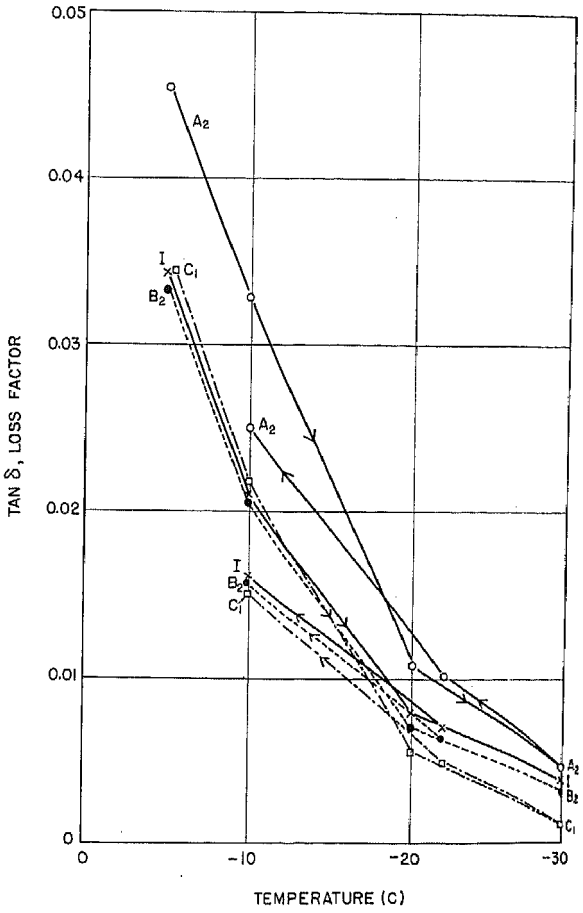

Figure 44. Hysteresis phenomenon in the relation between loss factor and temperature.

Activation energy. The logarithm of viscosity calculated by using the Maxwell model was plotted against the reciprocal of the absolute temperature, and it was found that a linear relationship held for each of the samples (Fig. 45). The datum for C1 ice at -5C is the only exception, and is excluded in this discussion. The relation is expressed by

$$\eta = \text{Const. } \exp\left(+\frac{F}{RT}\right), \qquad (21)$$

in which F is the activation energy, R the gas constant, T the absolute temperature. From the slope of the line, the activation energy is calculated as follows:

F = 12.7 kcal/mol for commercial ice,

F = 13.5 kcal/mol for superimposed ice A2,

F = 13.9 kcal/mol for ice with elongated bubbles B2,

F = 18.7 kcal/mol for ice with small bubbles C1 and C2.

The activation energy of C1 and C2 ice is considerably larger. It is considered that this ice, from a spot 680 ft from the entrance of the ice tunnel, is very old and has been under an intensive stress for a very long time. Judging from the size and shape of air bubbles, B2 ice must be much younger than C ice. The superimposed ice A2 is of course very new compared with B and C ice. It is an interesting phenomenon that the activation energy is larger for the older ice, although the density is almost the same for all these samples.

We adopted the Maxwell model in this calculation, but the value of the activation energy does not change if the Voigt model is employed. In that case the equation becomes

$$\eta = \text{Const. } \exp\left(-\frac{F}{RT}\right)$$

and the value of F remains the same.

Frequency dependence of loss factor and viscosity. The loss factor is plotted against frequency in Figure 46. The experiments at -10C were carried out more carefully than in the other cases. For ice cap samples B2 and C1, the loss factor decreases appreciably with increase in frequency within the range of 200 and 350 cps, but above

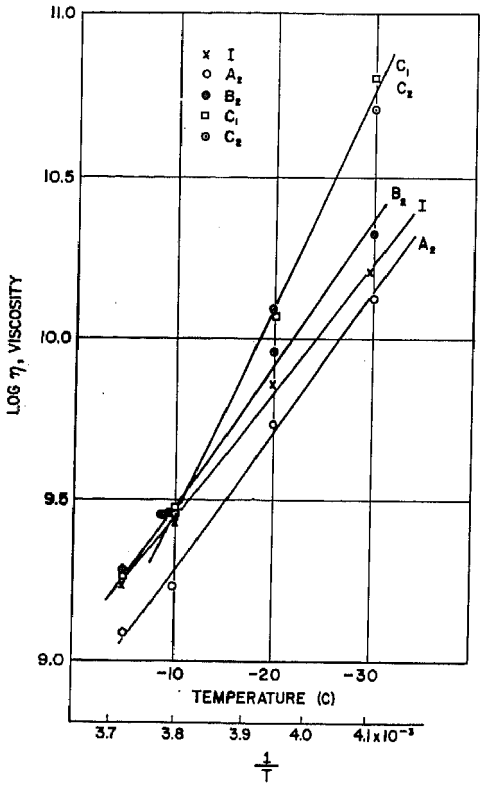

Figure 45. Log η vs temperature.

350 cps it is almost independent of frequency. The commercial ice follows the same course, but the frequency dependence of superimposed ice A2 is more marked.

Adopting the Maxwell model, Figure 46 is transformed into Figure 47, which shows the frequency dependence of viscosity. It is very interesting that the viscosity is almost constant in the wide range of frequency between 200 and 500 cps for tests at -10C, when the Maxwell model is used. The frequency was extended to 100 cps in the other experiments, and gradual decrease in viscosity with increase in frequency was observed within the range of lower frequencies. This curve is used for making the frequency correction of viscosity in the viscosity-density diagram (Fig. 49). Points P and Q which deviate considerably from the tan δ - f curve (Fig. 46) are on the η - f curve in Figure 47. This is due to the deviation in the value of E, which compensates for the deviation in tan δ (see eq 20).

13. Relation between viscosity and density

The loss factor is a function of density and frequency. The curves in Figure 35, drawn irrespective of density, show the

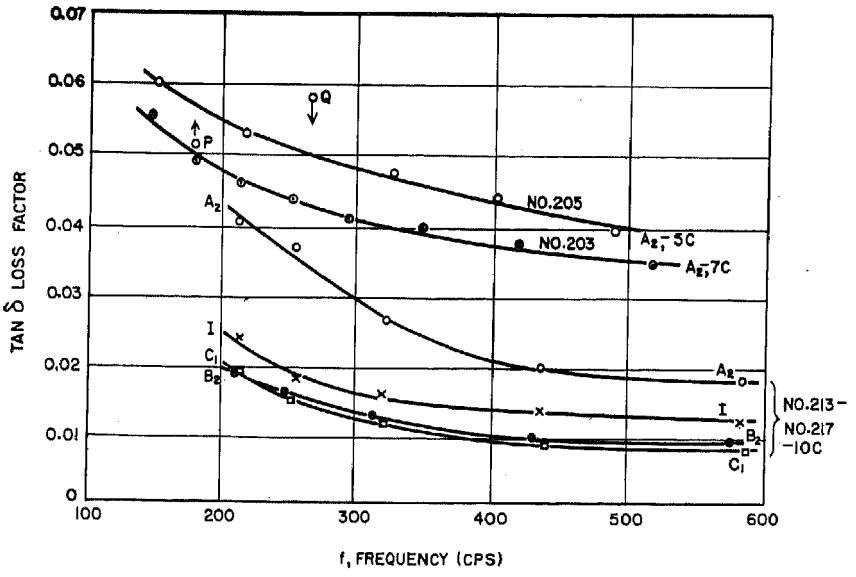

Figure 46. Frequency dependence of tan δ.

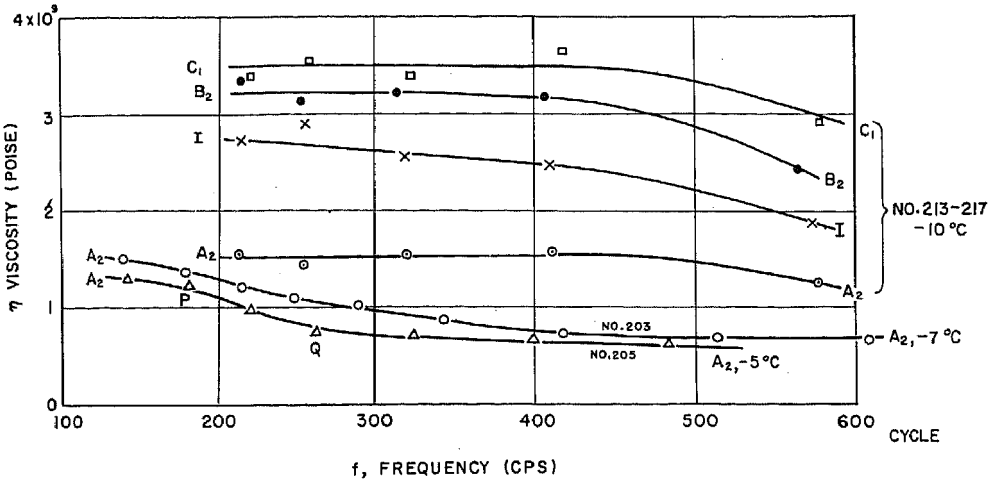

Figure 47. Frequency dependence of viscosity, Maxwell model.

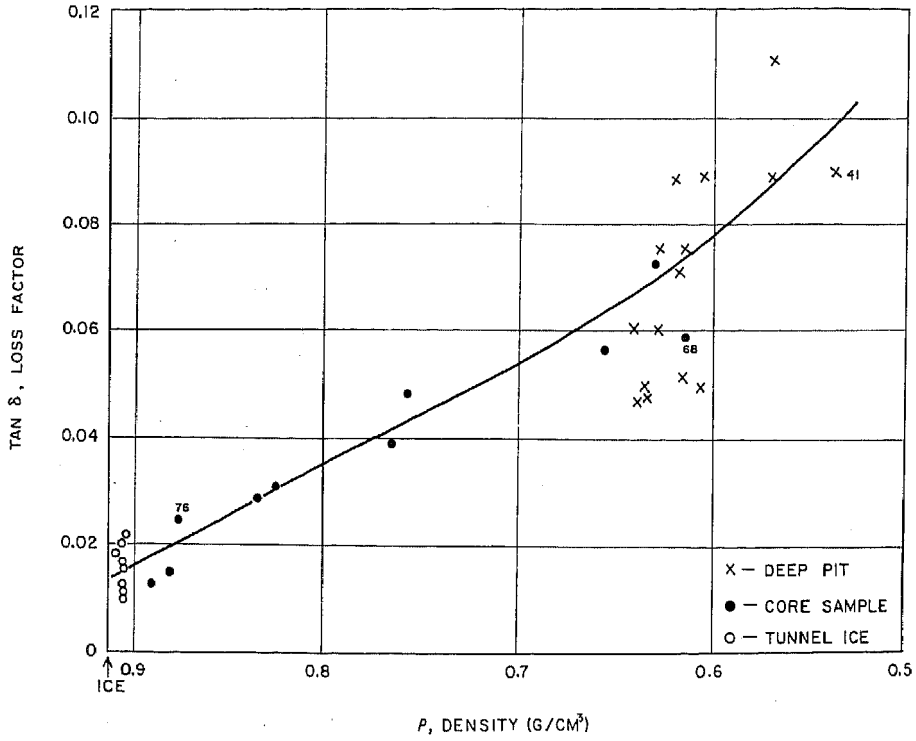

Figure 48. Loss factor vs density.
Temp -9C; frequencies above 250 cps.

superimposed effect of frequency and density. Figure 46 shows the frequency dependence for each of the samples, with density constant for each of the curves. For ice-cap samples B2 and C1, tan δ is constant within the error of ± 20% for frequencies above 250 cps. To get a rough idea of the relation between loss factor and density, the data above 250 cps are plotted in Figure 48. As the frequency correction is not made, the points are scattered in a wide range, but the tendency of the curve is well defined. From ice to the sample of density about 0.6 g/cm³, the loss factor increases linearly with decrease in density, and the rate of increase becomes larger below density 0.6 g/cm³.

The variation of the viscous nature as a function of density is more clearly seen when the viscosity coefficient of the Maxwell model is plotted against density, because the viscosity is constant in a wide range of frequency as shown in Figure 47. All available data are plotted irrespective of frequency in Figure 49, with the logarithm of viscosity as ordinate. The relation is expressed by the solid line. No frequency correction is necessary in the range of density above 0.58 g/cm³, the point marked by 41, because the frequency used is above 250 cps.

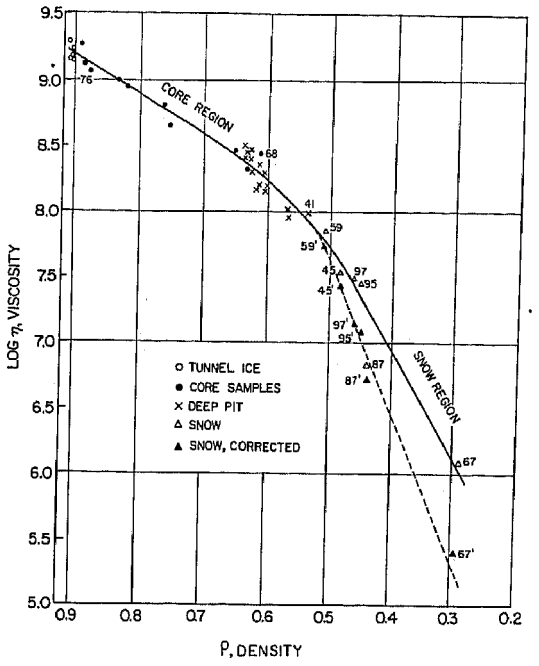

Figure 49. Viscosity vs density. Temp -9C, frequency between 200-400 cps.

In the range of density below about 0.5 g/cm³, that is, in the range of soft snow, the frequency varies between 105 and 222 cps. No data is available for the frequency dependence of snow samples in this range, but a tentative correction is made by assuming that the frequency dependence is similar to curves 203 and 205 in Figure 47, and calculating the value of η corresponding to frequencies between 200 and 400 cps. Within this range η is assumed to be independent of frequency in the case of snow samples also. The uncorrected values for snow samples are shown by white triangles in Figure 49, and the corrected values by dark triangles. If this correction is adequate, the log η-ρ relation for soft snow (densities below 0.538 g/cm³) will follow the broken line in Figure 49. Whether the correction is adequate or not, it is an established fact that log η decreases almost linearly with decrease in density until it reaches about 0.55 and that the rate increases for the lower densities. In the snow region, below 0.5 g/cm³ density, another linear relationship is observed with a steeper slope.

Comparing this result with the E - ρ relation in Figure 25 shows that Young's modulus and viscosity show similar behavior as a function of density. The area below density 0.9 g/cm³ is divided into two regions; the core region and the snow region. For both Young's modulus and viscosity, the relation with respect to density is different for these two regions. In the case of viscosity the core region is between the densities of 0.9 and 0.55 g/cm³, whereas it is between 0.9 and 0.50 g/cm³ for Young's modulus. The transition of one region to the other cannot be abrupt but must be gradual. The lower limit of the core region may be 0.50 or 0.55 g/cm³. The difference is not essential. The difference between the ice region and the core region is not clearly seen in the value of viscosity, although it is marked in the case of Young's modulus.

14. Conclusions

A Young's modulus-density relation obtained for the whole range of snow and ice observable in the Greenland Ice Cap shows that the whole area is divided into three regions. In region I (tunnel ice), density between 0.917 and 0.90 g/cm³, Young's modulus

decreases very rapidly when the density deviates slightly from that of pure ice. Region I covers the range of density 0.90 to 0.50 g/cm^3 (samples from deep pit and drill cores). The relation between Young's modulus and density for the whole range of this region is expressed by a straight line of the form

$$E = (16.4\,\rho - 7.20) \times 10^{10}.$$

In region III (snow near the surface of the ice cap) Young's modulus decreases in an exponential form as the density decreases. The empirical formula is

$$E = C \exp\{-k(0.50 - \rho)\}.$$

k, a factor determined by the structure of snow, is 6.35 for ordinary settled snow and the empirical formula is

$$\log E = 6.80 + 6.35\,\rho.$$

The structure factor of wind-packed snow is smaller than that of ordinary settled snow, and for the granular snow the reverse is the case. If the structure of snow is examined by making thin sections and is correlated to k, this structure factor can be introduced effectively into snow mechanics. The physical interpretation of this $E - \rho$ relation for the whole range of ice and snow will be one of the important problems in the future.

Both Young's modulus and the loss factor are functions of temperature and frequency. Young's modulus showed a slight increase as the temperature was decreased. The loss factor decreased very rapidly with lower temperature. Adopting the Maxwell model, the loss factor $\tan\delta$ was converted into the coefficient of viscosity η by the following equation

$$\eta = \frac{E}{\omega \tan\delta}$$

in which ω is the angular frequency. η increases in an exponential form with decrease in temperature, and $\log\eta$ is expressed by a straight line when plotted as the function of $1/T$, T being the absolute temperature.

$$\eta = \text{Const.}\ \exp\left(+\frac{F}{RT}\right).$$

F is the activation energy, R the gas constant. From the slope of the line, the activation energy is calculated as follows.

F = 12.7 kcal/mol for commercial ice,
F = 13.5 kcal/mol for superimposed ice taken at TUTO,
F = 13.9 kcal/mol for the tunnel ice with elongated bubbles,
F = 18.7 kcal/mol for the ice taken at 680 ft from the portal of the ice tunnel.

The frequency dependence of Young's modulus is complicated, but not very large. For the loss factor, the effect is considerable, and no simple relation is observed between $\tan\delta$ and ρ, when the data are plotted irrespective of the frequency used. However, the frequency dependence becomes very small when viscosity η is used instead of the loss factor. A simple relation, therefore, is obtained when η is plotted against density. $\log\eta$ decreases almost linearly with decrease in density until it reaches about 0.55 g/cm^3 and the rate increases for the lower densities. In the snow region; that is, below 0.5 g/cm^3 of density, another linear relationship is observed with the steeper slope. Comparing this result with $E - \rho$ relation, it is noted that Young's modulus and viscosity show similar behavior as the function of density. From these results it is concluded that the visco-elastic meter, using the sonic method, is a powerful tool for the study of elastic and viscous nature of snow and ice in the Greenland Ice Cap.

REFERENCES

Butkovich, T. R. (1959) Some physical properties of ice from the TUTO tunnel and ramp, Thule, Greenland, U. S. Army Snow Ice and Permafrost Research Establishment, Corps of Engineers, Research Report 47.

deQuervain, M. (1946) Kristallplastiche Vorgänge im Schneeaggregat II (Crystallo-plastic phenomena in the snow aggregate. II), Interner Ber. no. 24, Eidg. Institute fur Schnee- und Lawinenforsch, (Davos-Switz.), 41p. (Text in German).

Fuchs, A. (1956) Preparation of plastic replicas and thin sections of snow, Snow Ice and Permafrost Research Establishment, Corps of Engineers, U. S. Army, Technical Report 41, 12p.

———— (1959) Some structural properties of Greenland snow, U. S. Army Snow Ice and Permafrost Research Establishment, Corps of Engineers, Research Report 42. (In preparation.)

Glen, J. W. (1952) Experiments on the deformation of ice, Journal of Glaciology, vol. 2, p. 111-114.

———— and Perutz, M. F. (1954) The growth and deformation of ice crystals, Journal of Glaciology, vol. 2, p. 397-403.

Griggs, D. T. and Coles, N. E. (1954) Creep of single crystals of ice, Snow Ice and Permafrost Research Establishment, Corps of Engineers, U. S. Army, SIPRE Report 11, 24p.

Jellinek, H. H. G. and Brill, R. (1956) Visco-elastic properties of ice, Journal of Applied Physics, vol. 27, p. 1198-1209.

Kuroiwa, D. and Yamaji, K. (1956) Study of elastic and viscous properties of snow by the vibration method, II, Teion Kagaku, A, vol. 15, p. 43-57.

Landauer, J. K. (1955) Stress-strain relations in snow under uniaxial compression, Journal of Applied Physics, vol. 26, p. 1493-1497.

Nakaya, U. (1956) Properties of single crystals of ice revealed by internal melting, Snow Ice and Permafrost Research Establishment, Corps of Engineers, U. S. Army, Research Paper 13, 86p.

Staverman, A. J. and Schwarzi, F. (1956) "Linear deformation behavior of high polymers" in Die Physik der Hochpolymeren (Physics of high polymers). Berlin: Springer-Verlag, Bd. 4, p. 23-33.

Steinemann, Samuel (1954) Results of preliminary experiments on the plasticity of ice crystals, Journal of Glaciology, vol. 2, p. 404-412.

Strutt, J. W. (Lord Rayleigh) (1925) Theory of sound. London, vol. 1, p. 273-278.

Yamaji, Kenji and Kuroiwa, Daisuke (1954) Study of elastic and viscous properties of snow by the vibration method, I, Teion-kagaku, A, vol. 13, p. 49-57. (Text in Japanese).

Yosida, Z., et. al. (1956) Physical studies of deposited snow, II, Contributions from the Institute of Low Temperature Science, Hokkaido University, no. 9, p. 37-40.

GPO 820886-3